

**SILVER NANOSTRUCTURE SENSOR FOR DETECTION
OF PPB CONCENTRATION HYDROGEN SULFIDE GAS**

BY

SOMPHON TRIPAN

**A THESIS SUBMITTED IN PARTIAL FULFILLMENT OF
THE REQUIREMENTS FOR THE DEGREE OF MASTER OF
ENGINEERING (ENGINEERING TECHNOLOGY)
SIRINDHORN INTERNATIONAL INSTITUTE OF TECHNOLOGY
THAMMASAT UNIVERSITY
ACADEMIC YEAR 2015**

**SILVER NANOSTRUCTURE SENSOR FOR DETECTION
OF PPB CONCENTRATION HYDROGEN SULFIDE GAS**

BY

SOMPHON TRIPAN

**A THESIS SUBMITTED IN PARTIAL FULFILLMENT OF
THE REQUIREMENTS FOR THE DEGREE OF MASTER OF
ENGINEERING (ENGINEERING TECHNOLOGY)
SIRINDHORN INTERNATIONAL INSTITUTE OF TECHNOLOGY
THAMMASAT UNIVERSITY
ACADEMIC YEAR 2015**



SILVER NANOSTRUCTURE SENSOR FOR DETECTION OF PPB
CONCENTRATION HYDROGEN SULFIDE GAS

A Thesis Presented

By
SOMPON TRIPAN

Submitted to
Sirindhorn International Institute of Technology
Thammasat University
In partial fulfillment of the requirements for the degree of
MASTER OF ENGINEERING (ENGINEERING TECHNOLOGY)

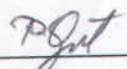
Approved as to style and content by

Advisor and Chairperson of Thesis Committee



(Asst. Prof. Paiboon Sreearunothai, Ph.D.)

Committee Member and
Chairperson of Examination Committee



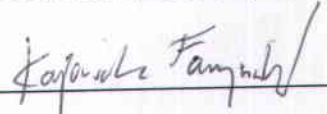
(Assoc.Prof. Pakorn Opaprasit, Ph.D.)

Committee Member



(Assoc.Prof. Thawatchai Onjun, Ph.D.)

Committee Member



(Dr. Kajornsak Faungnawakij, Ph.D.)

MARCH 2016

Acknowledgements

This dissertation would not have been possible without helps and supports from so many kind people around me. First of all, I would like to highly appreciate my principle advisor Asst. Prof. Paiboon Sreearunothai, Ph.D., School of Bio-Chemical Engineering and Technology (BCET), Sirindhorn International Institute of Technology (SIIT), Thammasat University for his kindly guidance, advices, supports, and encouragement. I also grateful to thank my co-advisor, Mr.Rungroj Maolanon, Researcher of Integrated Nanosystem Laboratory, National Nanotechnology Center (NANOTEC), National Science and Technology Development Agency (NSTDA) for giving me supports, guidance, advices. In addition, I would like to highly appreciate Thailand Advanced Institute of Science and Technology (TAIST-Tokyo Tech), Sirindhorn International Institute of Technology (SIIT), Integrated Nanosystem Laboratory, National Nanotechnology Center (Nanotec), National Science and Technology Development Agency (NSTDA) for grant supports, without this my dissertation not has been possible.

I would also like to appreciate committees, Assoc. Prof. Pakorn Opaprakasit, Ph.D., School of Bio-Chemical Engineering and Technology (BCET), Assoc.Prof. Thawatchai Onjun, Ph.D., School of Manufacturing Systems and Mechanical Engineering (MSME), Sirindhorn International Institute of Technology (SIIT), Thammasat University , and Dr. Kajornsak Faungnawakij, a prominent researcher at the National Nanotechnology Center (NANOTEC), National Science and Technology Development Agency (NSTDA), who are really kind to me, giving me great comments which very useful for my thesis.

In addition, I would like to thank Ajarn Ball who encouraged me to continue master degree. He always pushes me forward. I would also like to thank Ajarn Kanticha. She convinced my dad to permit me continue master degree. She had signed on the contract to be my guarantor. Thank you so much for believing in me. Without two of truly kind persons, this work and my master degree life might not have been happened. Particularly, Thank you mommy, dad and my beloved siblings for always be by my side. Thank you mommy for allowing me to borrow your car. Thank you dad for grant support. I love you guys. Thank you my lovely friends, my TAIST-Tokyo tech friends, all of friends who are always support me. Thank you so much for always listen to me when I am feeling blue.

Abstract

SILVER NANOSTRUCTURE SENSOR FOR DETECTION OF PPB CONCENTRATION HYDROGEN SULFIDE GAS

by

SOMPHON TRIPAN

Bachelor of Computer Engineering, Thai-Nichi Institute of Technology, 2013
Master of Engineering (Engineering Technology), SIIT, Thammasat University,
2015

Hydrogen sulfide occurs in crude oil petroleum, natural gas, hot spring, foods, and industries especially gas separation plant. It is one of the harmful toxic gases to human and its odor, even at concentration as low as 10 ppb, can already affect nearby communities. Most commercial hydrogen sulfide sensors have detection limit in the ppm range. Here, we report fabrication of gas sensor based on silver nanostructure capable of detecting hydrogen sulfide at concentration in the ppb and the ppm range. The sensor is fabricated by sputtering metallic silver onto silicon substrate forming a conductive channel with varying gap length between two electrodes also made from silver. The reaction of hydrogen sulfide with silver causes reduction in conductivity of the silver across the electrodes. The concentration of hydrogen sulfide gas was varied; 50 ppb, 100 ppb, 500 ppb, 1 ppm, 100 ppm, 300 ppm, 500 ppm at ambient conditions. The morphology of the silver nanostructured before and after exposed to hydrogen sulfide gas was investigated by FE-SEM, EDS and AES. The XRD studies further showed that sulfur compounds formed after exposure to the hydrogen sulfide gas was Silver sulfide. The sensor was found to be very selective to hydrogen sulfide, and no significance responses to other gases such as water, toluene, acetone, and chloroform were observed.

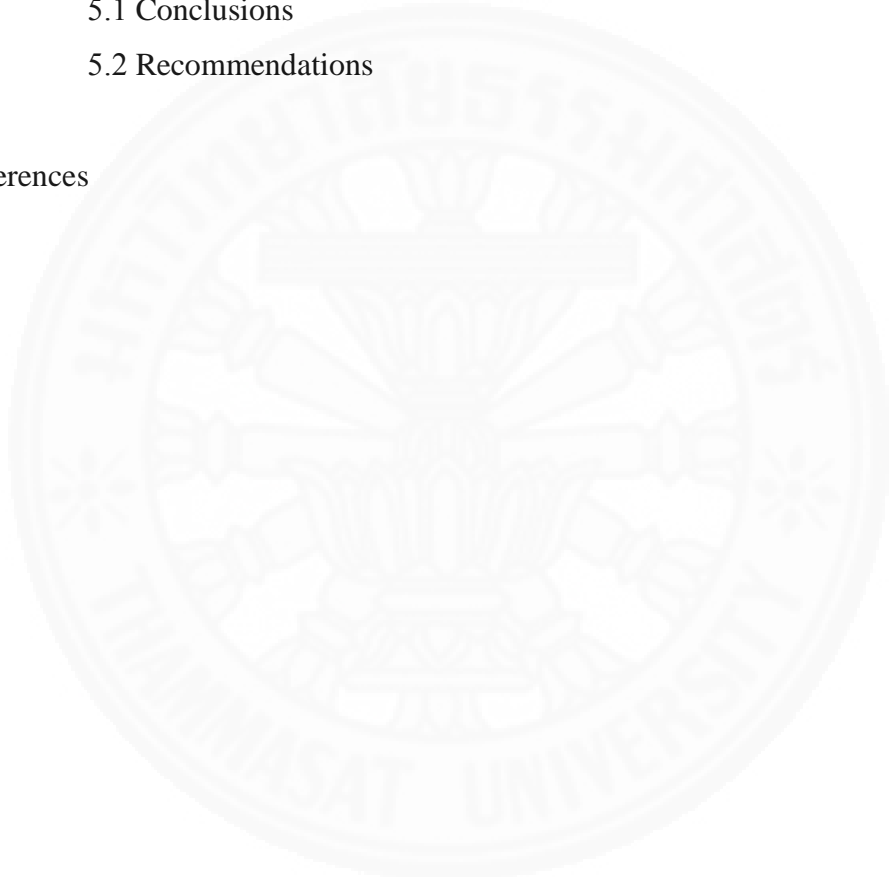
Keywords: Silver nanostructure, Hydrogen sulfide gas sensor, Nanoparticle

Table of Contents

Chapter	Title	Page
	Signature Page	i
	Acknowledgements	ii
	Abstract	iii
	Table of Contents	iv
	List of Tables	vii
	List of Figures	viii
1	Introduction	
	1.1 Introduction	1
	1.2 Statement of problems	2
	1.3 Objectives of study	2
	1.4 Scope of the study	3
2	Literature Review	4
	2.1 Hydrogen sulfide gas	4
	2.1.1 Source	4
	2.1.2 Environment and health effects	4
	2.1.2.1 Health effects	4
	2.1.2.2 Environmental effects	5
	2.1.3 Emission standard in Thailand	6
	2.1.4 Recommendations for hydrogen sulfide gas in workplace	6
	2.2 Gas sensors to detect hydrogen sulfide	6

2.2.1	Electrochemical sensors	7
2.2.2	Optical sensors	8
2.2.3	Conducting-polymer sensors	9
2.2.4	Semiconducting metal-oxide sensors	10
2.3	Silver nanostructure to detect hydrogen sulfide gas	14
2.3.1	Characterization of silver nanoparticles	15
2.3.2	Reaction between the silver and hydrogen sulfide gas	17
3	Experiments and method	18
3.1	Materials and chemicals	18
3.2	Experiments	18
3.2.1	Substrates preparation	18
3.2.2	Photolithography	18
3.2.3	Silver nanoparticles sputtering	20
3.2.4	Lift-off process	23
3.2.5	Gas exposure and interface experiments	24
3.2.5.1	Sensor exposure to hydrogen sulfide in the ppm range	25
3.2.5.2	Sensor exposure to hydrogen sulfide in the ppb range	25
3.2.6	Interference experiments	26
3.2.7	Characterization testing	26
4	Results and Discussion	27
4.1	Sensor fabrication results	27
4.1.1	Results of sensor fabrication in the preliminary phase	27
4.1.2	Results of sensor fabrication in the second phase	30
4.2	Characterizations of the silver nanostructure sensor	36
4.3	Responses of Ag nanostructure sensor to hydrogen sulfide and other gases	41
4.3.1	Responses of silver nanostructures sensor to hydrogen sulfide in the ppm range	43

4.3.2 Responses of silver nanostructures sensor to hydrogen sulfide in the ppb range	44
4.3.3 Investigation on interference from water vapor (air humidity), and other gases	57
5 Conclusions and Recommendations	65
5.1 Conclusions	65
5.2 Recommendations	65
References	67



List of Tables

Tables	Page
2.1 Representative conducting polymers	10
2.2 Interplanar distances (d-spacings) for electron diffraction patterns of silver nanoparticles and silver sulfide nanoparticles	17
3.1 Sputtering conditions for the titanium adhesive layer	22
3.2 Sputtering conditions for the silver electrode layer	23
3.3 Sputtering conditions for the sensing layer (sensing silver wire)	23
3.4 Ratio between chemical precursors (FeS and HCl (37%))	25
3.5 Dilution of the 150-ppm hydrogen sulfide gas in the 6,900 cm ³ desiccator chamber	26
4.1 Resistances of the sensors for preliminary phase from calculations and from measurements	28
4.2 The resistances of the sensors for the second-experiment (lot 1) from calculations and measurements	32
4.3 Resistances of the sensors for second-experiment (lot 2) from calculations and measurements	34
4.4 EDS result of silver nanoparticles 5 nm thick on the substrate after exposed to hydrogen sulfide gas	39

List of Figures

Figures	Page
2.1 Basic of electrochemical sensor	7
2.2 Schematic of sensor structure based on H ₂ SO ₄ pre-treated Nafion membrane as solid polymer electrolyte	7
2.3 Electrochemical sensors for real-time detection of hydrogen sulfide gas	8
2.4 IR-source gas sensors (a) based on the basic absorption spectrometry and (b) with reference filter/detector	9
2.5 Optical sensors for real-time detection of hydrogen sulfide gas	9
2.6 Conducting polymer sensors (CPSs) for real-time detection of hydrogen sulfide gas	10
2.7 Schematics and band diagrams showing before and after CuO films are exposed to hydrogen sulfide gas at various concentrations. (a) Mechanism in air before exposing, (b) when CuO films are exposed to hydrogen sulfide at low concentration, (c) when CuO film are exposed to hydrogen sulfide gas at high concentration	11
2.8 The responses of CuO films to hydrogen sulfide gas at various concentrations. (a) Low concentration (100-400 ppb), (b) intermediate concentration (500 ppb to 50 ppm), and (c) high concentration (more than 50 ppm).	12
2.9 The response of ZnO nanorods with flower-like structure sensor. When hydrogen sulfide was injected in the measurement system, the resistance decreases. Decreasing of resistance depends on the concentration of hydrogen sulfide gas which it is showed in figure, resistance of sensor at hydrogen sulfide 5 ppm decrease more than response of sensor at hydrogen sulfide 1 ppm	13
2.10 Semiconducting metal-oxide sensors for real-time detection of hydrogen sulfide gas	13
2.11 Comparisons of basic criteria across different sensor types of hydrogen sulfide gas (a) response time comparison, and (b) detection limit values	14

2.12 (a) AFM image of silver film fabricated by using DC-magnetron sputtering at room temperature with pure argon gas in chamber. (b) XRD spectra of silver films deposited at room temperature in various O ₂ content	16
2.13 Electron diffraction patterns of (a) silver nanoparticle films and (b) silver sulfide nanoparticles films	16
3.1 Dimensions of the silicon substrates used in (a) the preliminary-phase experiment, and (b) the second-phase experiment	19
3.2 Process for fabrication of the silver nanostructured sensor	21
3.3 Dimensions of the masks used for making (a) the electrode pattern and (b) the sensing wire pattern used in the preliminary-phase experiment. (c) 4 pairs of electrode patterns on a single substrate, and (d) the sensing wire pattern used in the second phase experiment	22
3.4 Schematic diagram of the measurement system for detecting the hydrogen sulfide and other gases	24
4.1 The example of sensor from the preliminary experiment. The gap between the electrodes is 100 μm (G100). The width of the sensing is 100 μm (W100). The sensor exposed to hydrogen sulfide effect on the changes of color from silver color to be yellow. For the preliminary experiment, the nanoparticles from sputtering process also appear around the side of substrate which they might connect with electrodes	27
4.2 Long term stability plots of silver nanostructured sensors of preliminary experiment for 15 days at ambient atmosphere. The gap between the electrodes is 50 μm (G50), and the width of the sensing wire is 50 μm (W50)	29
4.3 Long term stability plots of silver nanostructured sensors of preliminary experiment for 15 days at ambient atmosphere. The gap between the electrodes is 100 μm (G100), and the width of the sensing wire is 50 μm (W50)	29
4.4 Example of sensors from the new fabrication process. The gap between the electrodes is 100 μm (G100). The electrodes are made from the silver of 200 nm thick. The width of the sensing wire is 100 μm (W100) which is	

also made from the silver of 5 nm thick). (a) The finished sensors. One substrate contains 4 sensors. (b) The substrate was cracked to separate each sensor before use in gas exposure experiment	30
4.5 Long term stability plot of silver nanostructured sensors of the second-experiment (lot 1) for 30 days at ambient atmosphere. The gap between the electrodes is 50 μm (G50), and the width of the sensing wire was fixed at 100 μm (W100)	31
4.6 Long term stability plot of silver nanostructured sensors of second-experiment (lot 1) for 30 days at ambient atmosphere. The gap between the electrodes is 100 μm (G100), and the width of the sensing wire was fixed at 100 μm (W100)	33
4.7 Long term stability plot of silver nanostructured sensors of second-experiment (lot 1) for 30 days at ambient atmosphere. The gap between the electrodes is 500 μm (G500), and the width of the sensing wire was fixed at 100 μm (W100)	33
4.8 Long term stability plot of silver nanostructured sensors of the second-experiment (lot 2) for 30 days at ambient atmosphere. The gap between the electrodes is 50 μm (G50), and the width of the sensing wire was fixed at 100 μm (W100)	35
4.9 Long term stability plot of silver nanostructured sensors of second-experiment (lot 2) for 30 days at ambient atmosphere. The gap between the electrodes is 100 μm (G100), and the width of the sensing wire was fixed at 100 μm (W100).	35
4.10 Long term stability plot of silver nanostructured sensors of second-experiment (lot 2) for 30 days at ambient atmosphere. The gap between the electrodes is 500 μm (G500), and the width of the sensing wire was fixed at 100 μm (W100)	36
4.11 The FE-SEM images of (a) silver nanoparticles (b) silver nanoparticles after exposed to hydrogen sulfide gas for one hour at the concentration of 500 ppm. The thickness of the silver nanoparticle is five nanometers	36
4.12 The FE-SEM images focusing on sensing part of silver sensor (a) before exposure to hydrogen sulfide gas, (b) after exposed to hydrogen sulfide at	

100 ppm, (c) after exposed to hydrogen sulfide at 300 ppm, and (d) after exposed to hydrogen sulfide at 500 ppm. The images were taken at 700x magnifications	37
4.13 The FE-SEM images focusing on the sensing part of the silver sensor (a) before exposure to hydrogen sulfide gas, (b) after exposure to hydrogen sulfide at 100 ppm, (c) after exposure to hydrogen sulfide at 300 ppm, and (d) after exposure to hydrogen sulfide at 500 ppm. The images were taken at 10,000x magnification	38
4.14 XRD spectra of (a) silver nanoparticles 5 nm thick (b) silver nanoparticles 5 nm thick after expose to hydrogen sulfide gas and (c) XRD of silver sulfide pattern (PDF 00-002-0998).	40
4.15 Shows results of the depth profile analysis of (a) silver 50 nm thick and (b) silver 50 nm thick after exposed to hydrogen sulfide gas (700 ppm, 1h). Sulfur is found to about 5nm depth from the Ag top surface. The thickness of Ag film as read from the AES agrees very well with the thickness read from the QCM in the sputtering machine	41
4.16 An equivalent circuit of silver nanoparticles 5 nm thick between the silver nanoparticles 200 nm thick electrodes	42
4.17 Response of sensors to hydrogen sulfide gas at 300 ppm concentration, the gap between the electrodes were varied as 50 μm (G50), 100 μm (G100), and 500 μm (G500)	43
4.18 Responses of sensors (G100) to hydrogen sulfide gas at various concentrations; 100 ppm, 300 ppm, and 500 ppm	44
4.19 Responses of sensors (G50-W100) to hydrogen sulfide gas at 50 ppb concentration. The gap between the electrodes is 50 μm (G50). Width of sensing wire is 100 μm (W100)	45
4.20 Responses of sensors (G50-W100) to hydrogen sulfide gas at 100 ppb concentration. The gap between the electrodes is 50 μm (G50). Width of sensing wire is 100 μm (W100)	45
4.21 Responses of sensors (G50-W100) to hydrogen sulfide gas at 500 ppb concentration. The gap between the electrodes is 50 μm (G50). Width of sensing wire is 100 μm (W100)	46

4.22 Responses of sensors (G50-W100) to hydrogen sulfide gas at 1 ppm concentration. The gap between the electrodes is 50 μm (G50). Width of sensing wire is 100 μm (W100)	46
4.23 The average sensors responses of each concentration (G50-W100) to hydrogen sulfide gas at various concentrations: 50 ppb, 100 ppb, 500 ppb, and 1 ppm. The gap between the electrodes is 50 μm (G50). Width of sensing wire is 100 μm (W100)	47
4.24 Responses of sensors (G100-W100) to hydrogen sulfide gas at 50 ppb concentration. The gap between the electrodes is 100 μm (G100). Width of sensing wire is 100 μm (W100)	49
4.25 Responses of sensors (G100-W100) to hydrogen sulfide gas at 100 ppb concentration. The gap between the electrodes is 100 μm (G100). Width of sensing wire is 100 μm (W100)	49
4.26 Responses of sensors (G100-W100) to hydrogen sulfide gas at 500 ppb concentration. The gap between the electrodes is 100 μm (G100). Width of sensing wire is 100 μm (W100)	50
4.27 Responses of sensors (G100-W100) to hydrogen sulfide gas at 1 ppm concentration. The gap between the electrodes is 100 μm (G100). Width of sensing wire is 100 μm (W100)	50
4.28 The average sensors responses of each concentration (G100-W100) to hydrogen sulfide gas at various concentrations: 50 ppb, 100 ppb, 500 ppb, and 1 ppm. The gap between the electrodes is 100 μm (G100). Width of sensing wire is 100 μm (W100)	51
4.29 Responses of sensors (G500-W100) to hydrogen sulfide gas at 50 ppb concentration. The gap between the electrodes is 500 μm (G500). Width of sensing wire is 100 μm (W100)	52
4.30 Responses of sensors (G500-W100) to hydrogen sulfide gas at 100 ppb concentration. The gap between the electrodes is 500 μm (G500). Width of sensing wire is 100 μm (W100)	52
4.31 Responses of sensors (G500-W100) to hydrogen sulfide gas at 500 ppb concentration. The gap between the electrodes is 500 μm (G500). Width	

of sensing wire is 100 μm (W100)	53
4.32 Responses of sensors (G500-W100) to hydrogen sulfide gas at 1 ppm concentration. The gap between the electrodes is 500 μm (G500). Width of sensing wire is 100 μm (W100)	53
4.33 The average sensors responses of each concentration (G500-W100) to hydrogen sulfide gas at various concentrations: 50 ppb, 100 ppb, 500 ppb, and 1 ppm. The gap between the electrodes is 100 μm (G500). Width of sensing wire is 100 μm (W100)	54
4.34 The average sensors responses to hydrogen sulfide gas at 50 ppb concentrations. The gaps between the electrodes were varied: 50 μm (G50), 100 μm (G100), and 500 μm (G500). Width of sensing wire is 100 μm (W100)	55
4.35 The average sensors responses to hydrogen sulfide gas at 100 ppb concentrations. The gaps between the electrodes were varied: 50 μm (G50), 100 μm (G100), and 500 μm (G500). Width of sensing wire is 100 μm (W100)	55
4.36 The average sensors responses to hydrogen sulfide gas at 500 ppb concentrations. The gaps between the electrodes were varied: 50 μm (G50), 100 μm (G100), and 500 μm (G500). Width of sensing wire is 100 μm (W100)	56
4.37 The average sensors responses to hydrogen sulfide gas at 1 ppm concentrations. The gaps between the electrodes were varied: 50 μm (G50), 100 μm (G100), and 500 μm (G500). Width of sensing wire is 100 μm (W100)	56
4.38 The responses of sensors to humidity. The humidity was varied: 20%, 40%, and 60%. The gap between the electrodes is 50 μm (G50). The sensing wire is 100 μm (W100)	58
4.39 The responses of sensors to humidity. The humidity was varied: 20%, 40%, and 60%. The gap between the electrodes is 100 μm (G100). The sensing wire is 100 μm (W100)	58
4.40 The responses of sensors to humidity. The humidity was varied: 20%,	

- 40%, and 60%. The gap between the electrodes is 500 μm (G500). The sensing wire is 100 μm (W100). 59
- 4.41 The responses of sensors to hydrogen sulfide compare to humidity. The humidity was varied: 20%, 40%, and 60%. Hydrogen sulfide gas was varied: 50 ppb, 100 ppb, 500 ppb, and 1 ppm. The gap between the electrodes is 50 μm (G50). The sensing wire is 100 μm (W100). 59
- 4.42 The responses of sensors to hydrogen sulfide compare to humidity. The humidity was varied: 20%, 40%, and 60%. Hydrogen sulfide gas was varied: 50 ppb, 100 ppb, 500 ppb, and 1 ppm. The gap between the electrodes is 100 μm (G100). The sensing wire is 100 μm (W100). 60
- 4.43 The responses of sensors to hydrogen sulfide compare to humidity. The humidity was varied: 20%, 40%, and 60%. Hydrogen sulfide gas was varied: 50 ppb, 100 ppb, 500 ppb, and 1 ppm. The gap between the electrodes is 500 μm (G500). The sensing wire is 100 μm (W100) 60
- 4.44 The responses of sensors to other gases: acetone, methanol, chloroform, dichloromethane (DCM), and toluene at 5,000 ppm. The gap between the electrodes is 50 μm (G50). The sensing wire is 100 μm (W100) 61
- 4.45 The responses of sensors to other gases: acetone, methanol, chloroform, dichloromethane (DCM), and toluene at 5,000 ppm. The gap between the electrodes is 100 μm (G100). The sensing wire is 100 μm (W100) 61
- 4.46 The responses of sensors to other gases: acetone, methanol, chloroform, dichloromethane (DCM), and toluene at 5,000 ppm. The gap between the electrodes is 500 μm (G500). The sensing wire is 100 μm (W100) 62
- 4.47 Responses of sensors (G50-W100) to hydrogen sulfide and other gases at time 30 min and ambient atmosphere. The concentration of hydrogen sulfide at 50 ppb, 100 ppb, 500ppb, 1,000 ppb(1 ppm) and the concentration of other gases at 5,000 ppm 62
- 4.48 Responses of sensors (G100-W100) to hydrogen sulfide and other gases at time 30 min and ambient atmosphere. The concentration of hydrogen sulfide at 50 ppb, 100 ppb, 500ppb, 1,000 ppb(1 ppm) and the concentration of other gases at 5,000 ppm 63
- 4.49 Responses of sensors (G500-W100) to hydrogen sulfide and other gases

at time 30 min and ambient atmosphere. The concentration of hydrogen sulfide at 50 ppb, 100 ppb, 500ppb, 1,000 ppb(1 ppm) and the concentration of other gases at 5,000 ppm. This shows a very high selectivity of the developed silver nano-sensor towards hydrogen sulfide gas

63



Chapter 1

Introduction

1.1 Introduction

Hydrogen sulfide (H_2S) is flammable gas, corrosive and well-known pollutants. It occurs both from human-made and natural processes such as crude oil petroleum, natural gas, hot springs, and sewage treatment plants. Industrial sources of hydrogen sulfide consist of natural gas plants, coke oven plants, petrochemical plants, tanneries, and food processing plants. Hydrogen sulfide is classified as a harmful toxic gas to human health. It causes skin burns, inflammation in eyes and respiratory diseases such as bronchitis, rhinitis and pneumonia [1-4]. People rapidly respond toward hydrogen sulfide even at the concentration as low as 0.47 ppb due to its strong odor.

Concentration of hydrogen sulfide that is considered to have an adverse effect on human health is given as 15 ppm for 10 min (short-term exposure), or 10 ppm for 8 hr. (long-term exposure) [5]. In addition to effects on human health, hydrogen sulfide gas in the ppb range can already cause damage to many materials especially metals [6-9]. To determine and investigate the gaseous pollutant in environment, the gaseous samples are usually determined by gas chromatography (GC)-based method. Nevertheless this method is not simple. It also required trained personnel to perform the measurement. The GC approach is not suitable for a short-time or on-site measurements [10].

Hydrogen sulfide gas sensors have been widely investigated and developed. Common sensor types for detecting hydrogen sulfide are semiconducting metal-oxide [11], electrochemical, optical, conducting polymer, quartz crystal microbalance and surface acoustic wave [10]. Semiconducting metal oxide sensors are widely used because of their simple construction, low power consumption, low weight and low cost. Widely used metal-oxide materials for H_2S gas detection are: SnO_2 [12, 13], ZnO [14], SnO_2-CuO [15, 16], Fe_2O_3 and CuO . Although metal-oxide sensors have been investigated generally, the limitations of metal-oxide

sensors are high temperature operation ($>160^{\circ}\text{C}$) and non-specificity. CuO films are reported to respond to hydrogen sulfide gas at the ppb range and at room temperature, but no report on specificity was given [17]. Metal nanostructures have also been investigated for hydrogen sulfide detection. For example silver nanoparticle films are used for optical sensing of hydrogen sulfide gas in the ppm rang at ambient conditions but [18] the system based on the optical detection is rather large and complex.

1.2 Statement of problems

Several hydrogen sulfide gas sensor technologies have been widely developed and investigated. Nevertheless, these sensors still have some limitations such as:

1. Commercial sensors with good selectivity to hydrogen sulfide gas still have high cost. Simple low cost sensors with high selectivity or performance is needed.
2. Commercial metal-oxide type sensors need to use high-temperature operation of at least 200°C , which may render these sensors unsafe in some situations or consume a lot of battery life. Sensors operating at ambient temperature would be desirable.

Therefore, the sensors to detect hydrogen sulfide or other pollutant gases at ambient conditions with simple construction, low cost, and easy operation are needed. To this, it was found that metal-nanostructure sensors for gas detection have not been widely investigated. Sensor based on metallic silver to detect hydrogen sulfide gas in ppb range has also not been reported. It is the objective of this work to carry out feasibility study on developing such sensors.

1.3 Objectives of study

According to the above introduction and discussion, purposes of this research are as follows:

- To make sensors for detecting hydrogen sulfide gas based on silver nanostructure

- To investigate efficiency of sensors such as responses, stability, sensitivity, and selectivity
- To investigate sensors for detecting hydrogen sulfide gas in ppb range
- To study further morphology and nanostructure of silver sensors.

1.4 Scope of the study

This study will investigate sensors based on silver nanostructure that are capable of detecting hydrogen sulfide at concentration in the ppm and ppb range at ambient conditions. The sensors will be fabricated by sputtering metallic silver onto a silicon substrate forming conductive channel with varying gap lengths between two silver electrodes. The reaction of hydrogen sulfide with silver causes reduction in conductivity of the silver across the sensing layer. The sensors will also be investigated for long-term stability, sensitivity, and selectivity. The morphology of the silver nanostructure before and after exposed to hydrogen sulfide gas will be investigated by an optical microscope, a transmission electron microscope (TEM), a field-emission scanning electron microscope (FE-SEM), and Auger electron spectroscopy (AES). Energy-dispersive X-ray spectrometer (EDS) is used to study the compositions of the silver sensing layer before and after exposure to the hydrogen sulfide gas. X-ray diffraction (XRD) is used further to confirm that the silver nanostructured sensor formed silver sulfide after the sensor exposed to the hydrogen sulfide gas.

Chapter 2

Literature review

2.1 Hydrogen sulfide gas

Hydrogen sulfide is colorless gas. Formula of hydrogen sulfide gas is H_2S with a characteristic odor of rotten eggs. Hydrogen sulfide is heavier than air. It is flammable, corrosive, poisonous, and explosive gas [19]. Usually, people notice a smell of hydrogen sulfide gas at low concentration in the air with ranging from 0.5 ppb to 0.3 ppm [20]. At high concentrations, people might lose ability to smell it. This is rather important because they might falsely think that no have hydrogen sulfide anymore. This is may increase their risk exposure [19].

2.1.1 Source

Hydrogen sulfide occurs in both from human-made and natural processes. It is in sulfur springs, gasses from volcanoes, undersea vents, crude oil, and natural gas [19]. From human-made processes such as petroleum refineries, petrochemical plants, natural gas plants, and coke oven plants [20]. Moreover, it is found in our mouth which it comes from bacteria and gastrointestinal produce hydrogen sulfide gas [20]. Hydrogen sulfide is also released from waste water treatment plants [20].

2.1.2 Environment and health effects

2.1.2.1 Health effects

Hydrogen sulfide enters through human body by breathing but at low concentrations can enter our body through the skin. Health effects of hydrogen sulfide gas depend on factors. For example, How much concentration we are exposed to and how long that exposure [20]. According to studies of toxicological profile for hydrogen sulfide report state no health effects have been found in people when they are exposed to hydrogen sulfide in typical environmental with concentration 0.11-0.33 ppb [19].

Respiratory effects

- At low concentrations of hydrogen sulfide may cause irritation to nose, eyes, or throat. People might difficulty in breathing.
- At high concentrations of hydrogen sulfide, people might distress or arrest their respiratory [19].

Nervous system

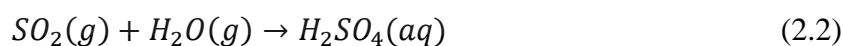
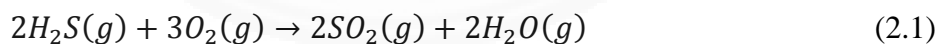
- At 2-20 ppm concentration of hydrogen sulfide may cause loss of appetite, headache, poor memory, and balance problems.
- At high concentrations of hydrogen sulfide as greater than 500 ppm can cause a loss of consciousness [19].

Hydrogen sulfide and cancer

- No have reports the cause of cancer in humans.
- The International Agency for Research on Cancer (IARC) and Department of Health and Human Services (DHHS) have not classified it as to its carcinogenicity.
- Environmental Protection Agency (EPA) also stated that hydrogen sulfide is not a carcinogen compound [19].

2.1.2.2 Environmental effects

The equation of acid rain from hydrogen sulfide gas



Hydrogen sulfide gas effects on the air pollutant. When it outs to the air, hydrogen sulfide reacts with O₂ formed sulfur trioxide. Then it becomes to be sulfuric acid or we all known in acid rain. It is corrosion in metallic [21]. It is not only effect on corrosive metallic. It is also effect on human and living on earth which it was mentioned in previous section.

2.1.3 Emission standard in Thailand

Industrial Emission standard for Hydrogen Sulfide (Any source)

Non-combustion : not exceeds 100 ppm

Combustion : not exceeds 80 ppm

Emission standard from Gas separation unit (Hydrogen Sulfide)

Not exceeds 60 ppm

2.1.4 Recommendations for hydrogen sulfide gas in workplace.

International standards

- Occupational Safety and Health Administration (OSHA) set an acceptable limit of hydrogen sulfide at 20 ppm in workplace air. The ceiling limit is 15 min.
- National Institute for Occupational Safety and Health (NIOSH) set an acceptable limit at 10 ppm with ceiling time 10 min. for workers [20].

Thailand standards

- Thailand occupational safety and health recommends a 10 min ceiling level of 20 ppm for workers.
- Thailand occupational safety and health also determined that 50 ppm is immediately dangerous to life or health to workers [20].

2.2 Gas sensors to detect hydrogen sulfide

Sensors for detecting hydrogen sulfide gas have been widely investigated because of its pollutant. Recently, real-time detecting sensors are needed such as metal-oxide sensor, electrochemical sensor, and optical sensor [5]. These sensors have their advantage and disadvantage such as fast response, high selectivity, high sensitivity, low cost, and easy operation depending on their materials and fabrication.

2.2.1 Electrochemical sensors

Electrochemical sensors start from 1950s. They have been widely investigated for gas monitoring. This kind of sensor also is used as commercial sensor because of their many advantages such as it is good for detecting of many different toxic gases, well sensitivity and selectivity. In addition, it consumes low power. For that reason, it is widely used in portable instrument which it contains many sensors. Figure 2.1 shows the basic of electrochemical sensor. The main part of electrochemical sensor is electrodes which they are made from different materials depending on target gases [22].

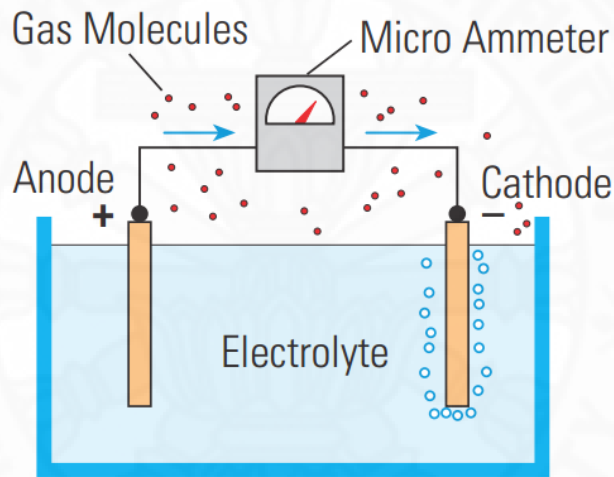


Figure 2.1 Basic of electrochemical sensor [22]

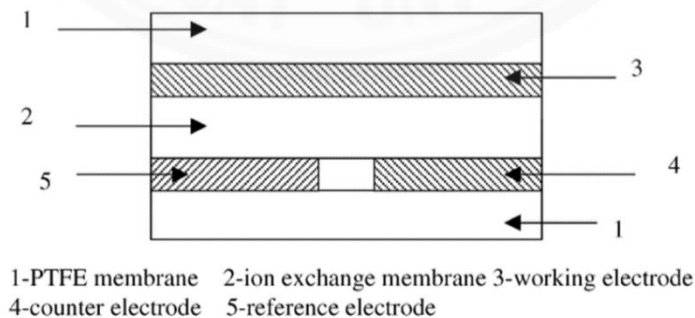


Figure 2.2 Schematic of sensor structure based on H_2SO_4 pre-treated Nafion membrane as solid polymer electrolyte

For example electrochemical to detect hydrogen sulfide, [23] Yu et al investigated electrochemical hydrogen sulfide gas sensor form H_2SO_4 pre-treated Nafion membrane as solid polymer electrolyte. They able to measure hydrogen sulfide gas with the range 1-100 ppm in a 9 s. response time. The lowest concentration that sensor able to measure is 0.1 ppm.

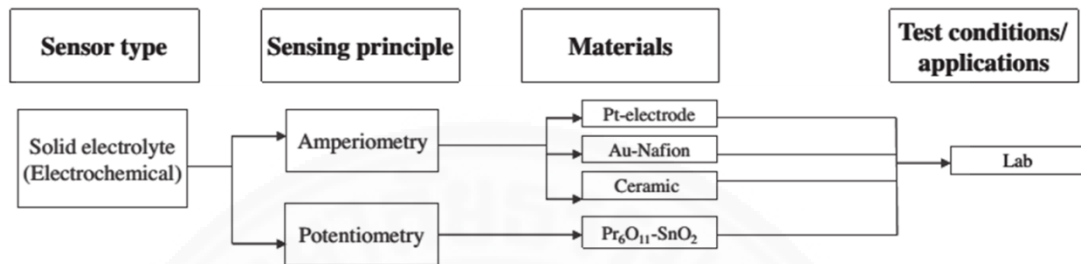


Figure 2.3 Electrochemical sensors for real-time detection of hydrogen sulfide gas.

2.2.2 Optical sensors

Optical sensors based on extenuation of light waves. The fabrication of these sensors frequently uses a waveguide and material coating. The results signal from this sensor comes from the absorption or emission phenomenon [10]. Advantages of this sensor are rather higher selectivity, sensitivity, and stability than others types with longer lifetime[24]. Mostly optical method for gas sensing based on spectroscopy. However, the cost of this method is quite high. There are many techniques based on absorption and emission spectrometry such as Differential Optical Absorption Spectroscopy (DOAS), Tunable Diode Laser Absorption Spectroscopy (TDLAS), Differential Absorption LIDAR (DIAL), Raman Light Detection and Ranging (LIDAL), Laser-Induced Breakdown Spectroscopy (LIBS), and Fourier Transform Infrared Spectroscopy (FTIR) [24].

Infrared (IR) is widely used to make gas sensors which are based on optical sensing. It is more specifically because several gases have own IR property with different wavelengths. Figure 2.4 shows the illustration of IR-source gas sensor (a) based on the basic absorption spectrometry and (b) with reference filter/detector. They contain major parts as IR source, gas chamber, and IR detector.

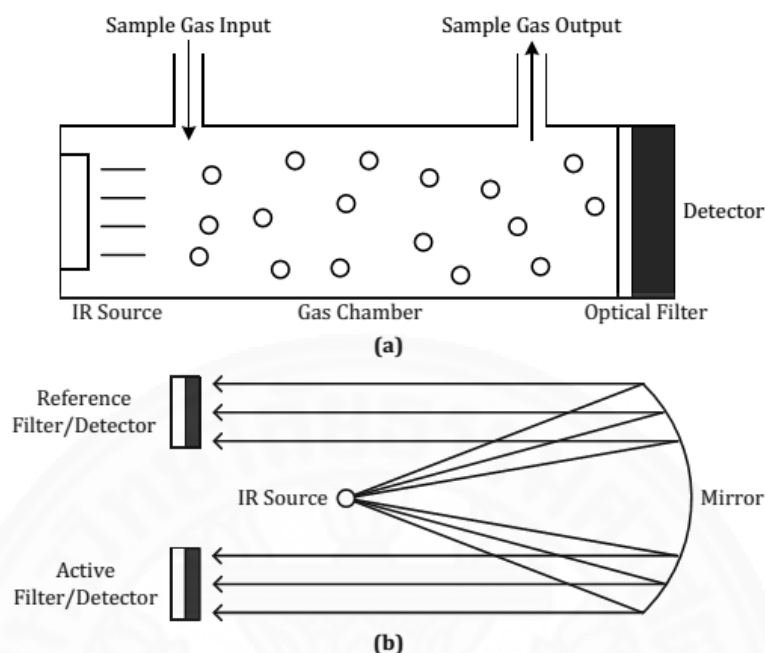


Figure 2.4 IR-source gas sensors (a) based on the basic absorption spectrometry and (b) with reference filter/detector.

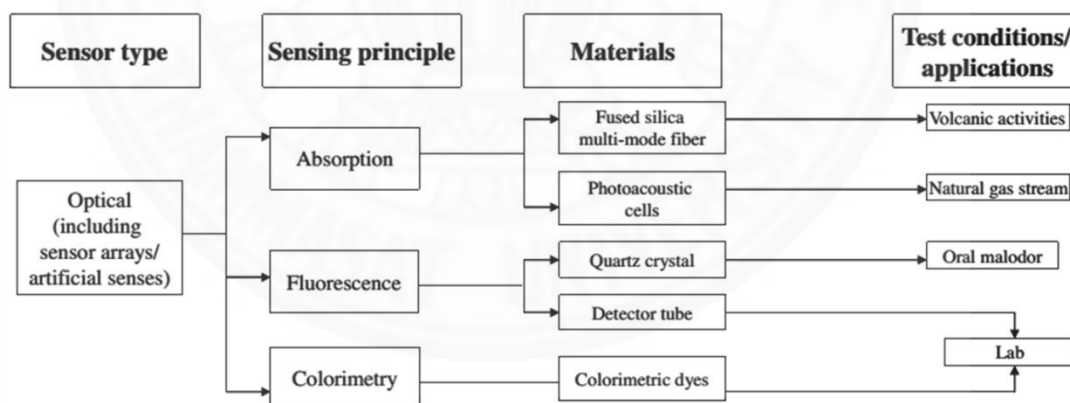


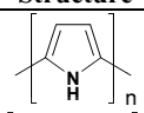
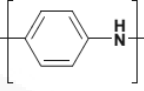
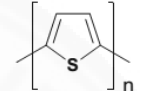
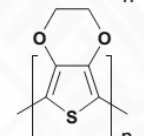
Figure 2.5 Optical sensors for real-time detection of hydrogen sulfide gas.

2.2.3 Conducting-polymer sensors

Because of their easy fabrication, conduction polymer sensors or CPSs broadly use for gas sensing. CPSs also have high reproducibility, fast reaction rate, and low price [25]. Basic idea of CPSs is the mixing of polymer selected for target gases with carbon nanotubes (CNTs), carbon black, multiple-walled carbon

nanotubes (MWCNTs)), and single-walled carbon nanotubes (SWCNTs). Table 2.1 shows the examples of conducting polymer [25].

Table 2.1 Representative conducting polymers.

Name	Structure
Polypyrrole (PPy)	
Polyaniline (PANI)	
Polythiophene (PTh)	
Poly(3,4-ethylenedioxythiophene) (PEDOT)	

The example of CPSs, the authors used polyaniline nanofibers and gold nanoparticles to increase the response of sensor. The sensors were fabricated by electrochemical technique. The electrodes of the sensor were gold in micron scale. Polyaniline nanowires were functionalized with gold nanoparticles by using voltammetry technique. The response time of the sensor was less than 120 s. The range of the response to hydrogen sulfide gas was 0.1-100 ppb with high selectivity and good reproducibility.

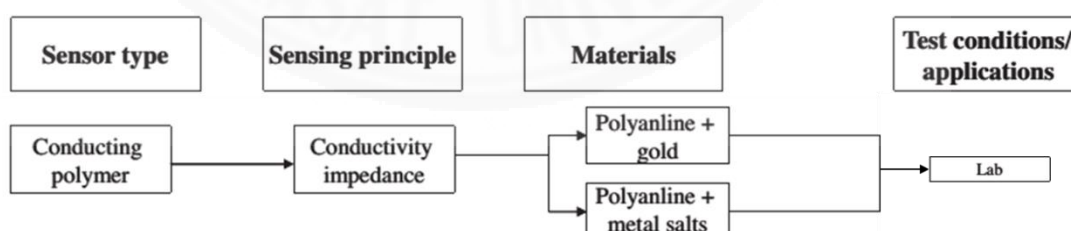


Figure 2.6 Conducting polymer sensors (CPSs) for real-time detection of hydrogen sulfide gas

2.2.4 Semiconducting metal-oxide sensors

Metal-oxide started from phenomenon of changes the conductivity of the material. Firstly, demonstration using zinc oxide thin film layer (1962) [26].

Metal oxide semiconducting sensors are in form of thick or thin film. It is based on metal-oxide materials such as ZnO, SnO₂, CuO, Fe₂O₃, WO₃, BaTiO₃, and In₂O₃ [10]. The sensors have many advantages as simple construction, small size, low power consumption, and cheap. However, to operate the sensor some of them need high temperature at least 160 °C. Because of their high temperature operation, many researchers have been developed the metal-oxide sensor to detect hydrogen sulfide at room temperature operation.

CuO thin film was investigated at room temperature to detect hydrogen sulfide gas. Their sensors were prepared by chemical vapor deposition. They found that the CuO films were highly sensitive towards hydrogen sulfide gas. They divided the concentration for three ranges as (a) low concentration (100-400 ppb), (b) intermediate concentration (500 ppb to 50 ppm), and (c) high concentration (more than 50 ppm). Mechanism of CuO films to hydrogen sulfide gas are represented in Figure 2.7 [17].

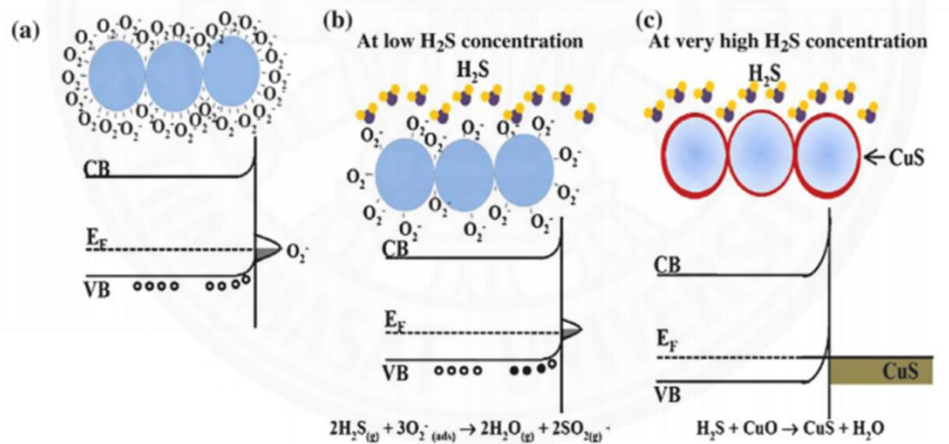


Figure 2.7 Schematics and band diagrams showing before and after CuO films are exposed to hydrogen sulfide gas at various concentrations. (a) Mechanism in air before exposing, (b) when CuO films are exposed to hydrogen sulfide at low concentration, (c) when CuO film are exposed to hydrogen sulfide gas at high concentration.

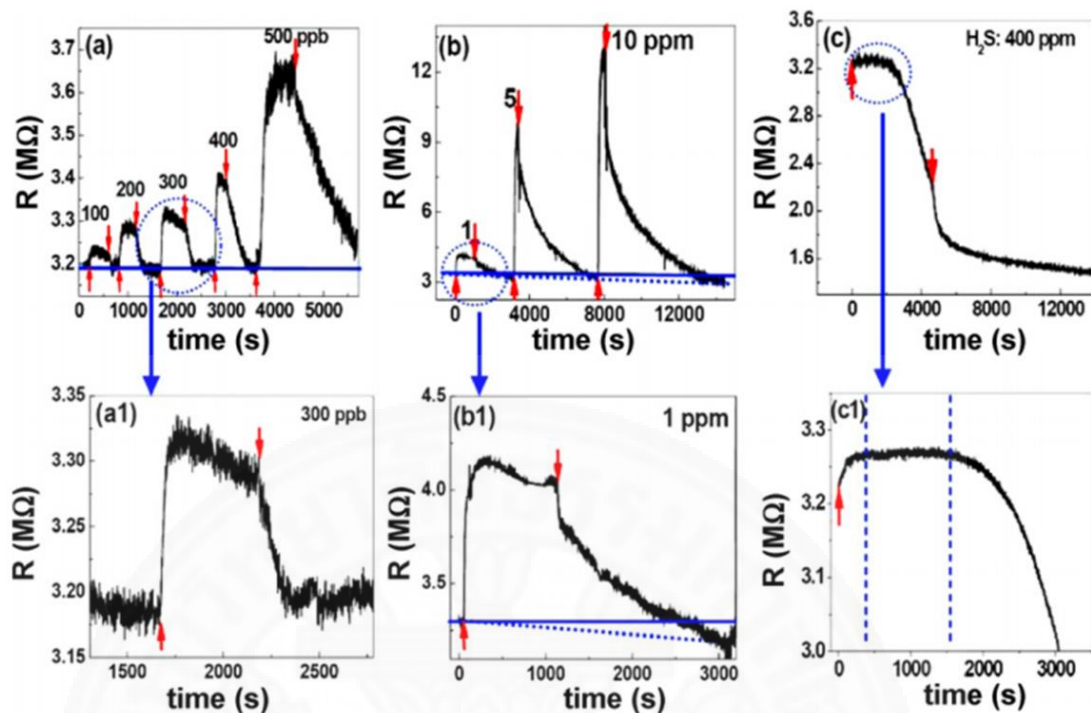


Figure 2.8 The responses of CuO films to hydrogen sulfide gas at various concentrations. (a) Low concentration (100-400 ppb), (b) intermediate concentration (500 ppb to 50 ppm), and (c) high concentration (more than 50 ppm).

Their result shows that their sensor responses to various concentrations of hydrogen sulfide gas at room temperature. The signal results are represented in Figure 2.8. ZnO is one of most metal-oxide that has been used to investigate pollutant gas detecting [26]. In 2014, it was investigated to detect hydrogen sulfide gas at room temperature [5]. ZnO rods were grown on quartz substrates by vapor phase transport method. The responses of the sensor based on rather aligned ZnO nanorods with flower-like structure were observed. The results found that the sensor able to detect hydrogen sulfide gas as low as 1 ppm to 5 ppm concentration of hydrogen sulfide [5]. The responses is showed as Figure 2.9

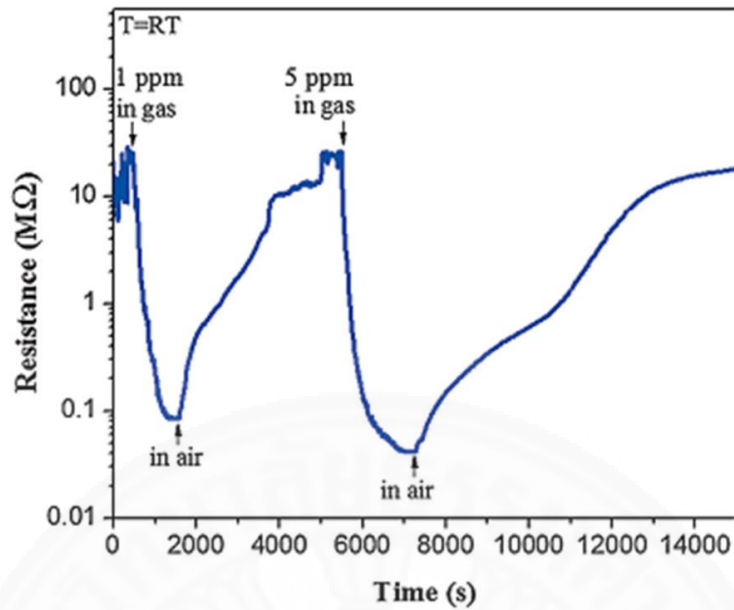


Figure 2.9 The response of ZnO nanorods with flower-like structure sensor. When hydrogen sulfide was injected in the measurement system, the resistance decreases. Decreasing of resistance depends on the concentration of hydrogen sulfide gas which it is showed in Figure, resistance of sensor at hydrogen sulfide 5 ppm decrease more than response of sensor at hydrogen sulfide 1 ppm [5].

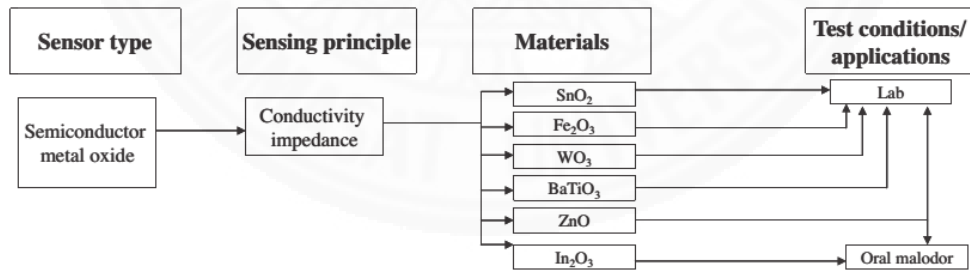


Figure 2.10 Semiconducting metal-oxide sensors for real-time detection of hydrogen sulfide gas

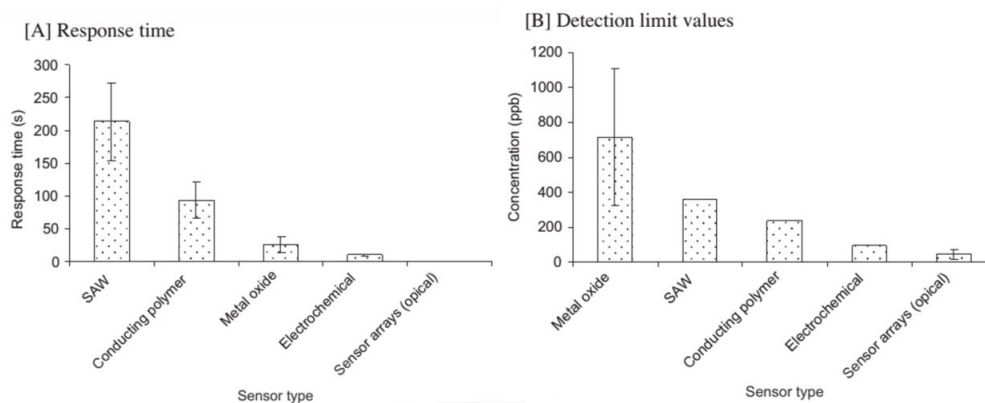


Figure 2.11 Comparisons of basic criteria across different sensor types of hydrogen sulfide gas (a) response time comparison, and (b) detection limit values.

2.3 Silver nanostructure to detect hydrogen sulfide gas

Silver nanostructured have been investigated for sensor, for example, silver nanoparticles were applied on single wall carbon nanotube to act as electrochemical sensor to detect hydrogen sulfide gas [22]. When silver is exposed to hydrogen sulfide gas formed silver sulfide [25]. Properties of silver also change effect on their resistance change. Therefore, it is impossible to apply this phenomenon for development of sensor to detect hydrogen sulfide gas based on silver nanoparticles [20].

In 2013, silver nanoparticle films were studied to detect hydrogen sulfide gas in ppm range at ambient condition. It is quite new that authors used metal to detect hydrogen sulfide. It is well known that silver rapidly reacts with hydrogen sulfide gas formed silver sulfide. Based on silver sulfide reaction, silver nanoparticle films were investigated in term to detect hydrogen sulfide gas by using optical property of silver nanoparticle films [20].

Silver nanoparticles films were fabricated on glass cuvettes by suspension of silver nanoparticles in water. The yellow films of silver nanoparticles were high 9 mm from the bottom of the cuvettes. To investigate the response of the films were exposed to hydrogen sulfide gas. Authors observed real-time of localized surface plasmon resonance (LSPR) absorption. The responses of sensor were measured by using peak intensity of LSPR [18]. The results showed that the silver

nanoparticles films are quite sensitive to hydrogen sulfide at low concentration as 1 ppm level. The limitation of this sensor is able to detect hydrogen sulfide 1 ppm to 20 ppm. If a concentration of hydrogen sulfide gas bigger than 20 ppm, the sensor cannot identify concentration. Further, this silver nanoparticles films very selectivity when it was exposed to others gases such as ammonia, hydrochloric acid, acetone, and ethanol. Other gases not significantly affected when compared with hydrogen sulfide gas [18].

2.3.1 Characterization of silver nanoparticles

Silver nanoparticles can fabricate by several ways. Sputtering technique also has been use to fabricate silver nanoparticles. W.M. Kim studied morphology of nanostructured silver thin films fabricated by DC-magnetron sputtering. Figure 2.12b shows the XRD spectra of silver films deposited in various O₂ contents at room temperature. XRD spectra of silver films at room temperature shows predominant peak (111) and a small peaks (200), (220), and (311). The morphology of silver films was more observed by AFM as shown in Figure 2.12a [27]. Figure 2.13a shows electron diffraction pattern of silver nanoparticles films prepared from suspension of silver nanoparticles in solution. Furthermore after the silver nanoparticle films were exposed to pure hydrogen sulfide, electron diffraction after exposed match well with the report of silver sulfide structure as shown in table 1 [28].

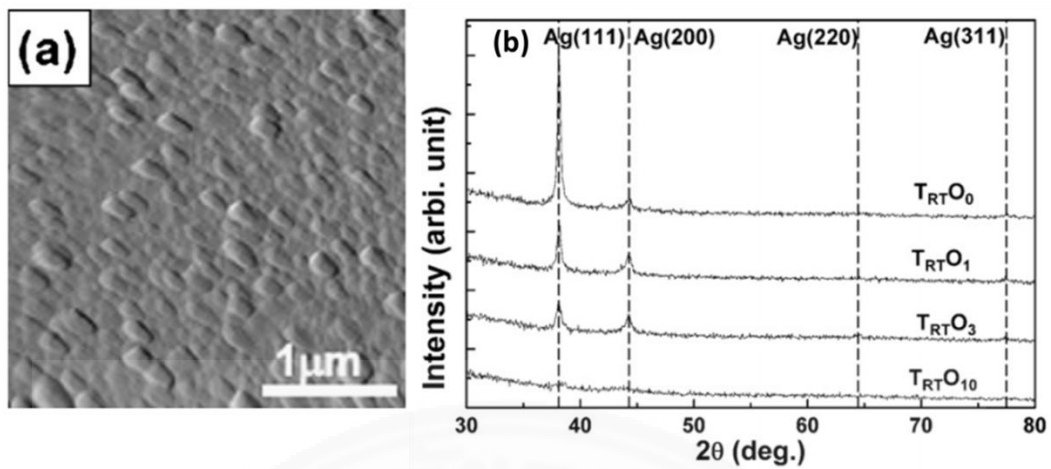


Figure 2.12 (a) AFM image of silver film fabricated by using DC-magnetron sputtering at room temperature with pure argon gas in chamber. (b) XRD spectra of silver films deposited at room temperature in various O_2 content.

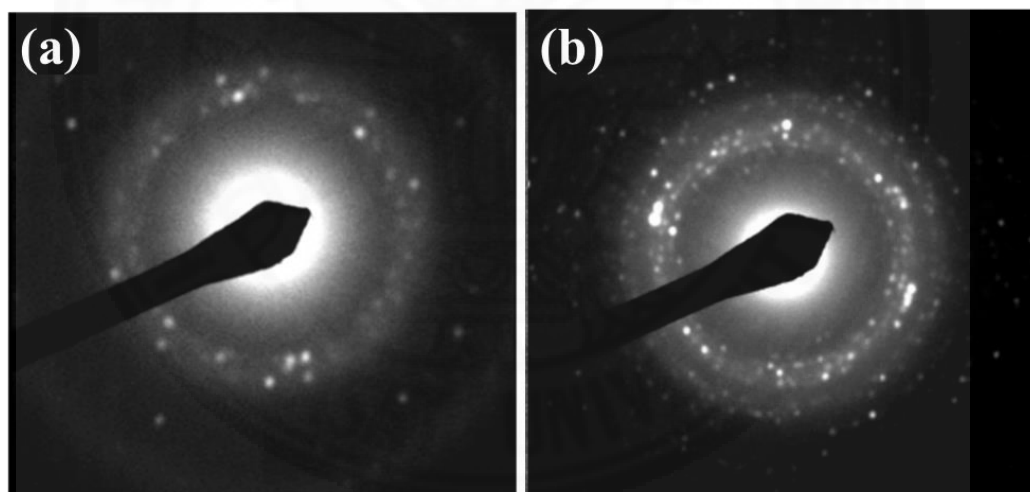


Figure 2.13 Electron diffraction patterns of (a) silver nanoparticle films and (b) silver sulfide nanoparticles films.

Table 2.2 Interplanar distances (d -spacings) for electron diffraction patterns of silver nanoparticles and silver sulfide nanoparticles.

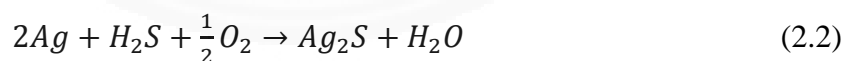
hkl	Ag (fcc)		hkl	Ag ₂ S (acanthite)	
	Measured (Å)	Reported (Å) ^a		Measured (Å)	Reported (Å) ^b
111	2.325	2.355	11 $\bar{1}$	3.456	3.437
200	2.016	2.039	012	3.404	3.383
220	1.423	1.442	111	3.053	3.082
222	1.175	1.177	11 $\bar{2}$	2.799	2.837
			12 $\bar{1}$	2.612	2.607
			022	2.555	2.583
			121	2.411	2.441
			10 $\bar{3}$	2.344	2.382
			031	2.181	2.214
			200	2.057	2.085

2.3.2 Reaction between the silver and hydrogen sulfide gas

Normally, the reaction between bulk silver and hydrogen sulfide gas is



Nevertheless, in general condition as atmospheric conditions. It contains O₂. Therefore the reaction is differently from 2.1. The reaction might present as



Chapter 3

Experiments and method

3.1 Materials and chemicals

- | | |
|--|--------------------------------|
| 1. Silicon wafer coated by SiO ₂ 200 nm thick | 10. Hydrogen sulfide (150 ppm) |
| 2. Photoresist: ma-P 125 | 11. Acetone |
| 3. Developer: ma-D 331 | 12. Methanol |
| 4. Silver (Target for sputtering process) | 13. Ethanol |
| 5. Titanium (Target for sputtering process) | 14. Propanol |
| 6. Iron sulfide (FeS) | 15. Toluene |
| 7. Aluminium sulfide (Al ₂ S ₃) | 16. Xylene |
| 8. Sodium sulfide (Na ₂ S) | 17. Dichloromethane (DCM) |
| 9. Hydrochloric acid (HCl) | 18. Chloroform |

3.2 Experiments

3.2.1 Substrates preparation

Silicon wafers were used for the sensor substrates. The top surface of the silicon wafers were coated with 200 nm of silicon dioxide (SiO₂). Substrates were cleaned by acetone, methanol, and propanol then they were dried by nitrogen gas. Two sizes of the substrates were used depending on experimental phase:

- (a) Preliminary phase: the size of the substrate was 10 mm. x 10 mm. x 0.5 mm.
- (b) Second phase: the size of the substrate was 26 mm. x 26 mm. x 0.5 mm.

3.2.2 Photolithography

Figure 3.2 shows the processes of photolithography. In Figure 3.2a, the photoresist (positive type, removed upon UV radiation) was applied to the cleaned substrate using 3,000 rpm of spin coater for one min. In Figure 3.2b, the substrate with the resist was then baked at 110 °C for 3 min. To create the pattern of the sensors, Figure 3.2c, the mask was put on the substrate with the resist layer, and then it was exposed to ultraviolet light for 0.5 sec. Figure 3.2c also shows the areas

for the two electrodes on both sides being exposed to UV light with the unexposed middle part as the gap between the two electrodes (cross sectional view). The sensing wire will be deposited across this gap (the remained part in the Figure 3.2d) connecting the two electrodes on both sides in the step shown in the Figure 3.2k.

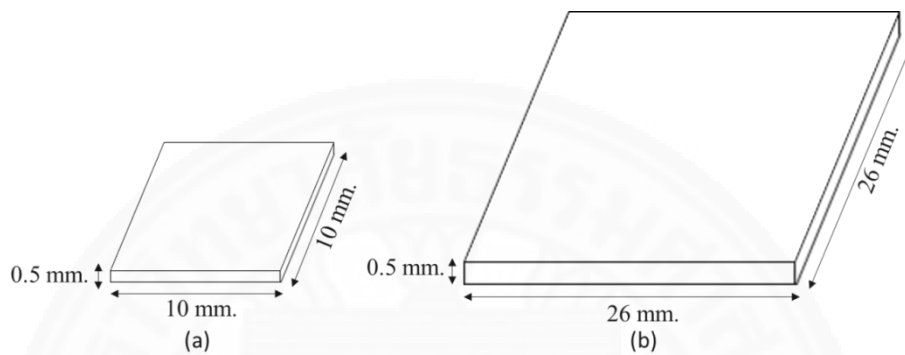


Figure 3.1 Dimensions of the silicon substrates used in (a) the preliminary-phase experiment, and (b) the second-phase experiment

In Figure 3.2d, the area of the resist which has been exposed to the UV light was removed by the developer (ma-331). The silver sputtering process and the lift-off process for making the electrodes of the sensor will be explained in the next section. The substrate with the silver electrodes was repeated with the photolithography process which are schematically represented in the Figure 3.2g – j. The mask arts for the electrode pattern and the sensing pattern were shown in Figure 3.3. Figure 3.3a shows the mask for making the electrode pattern. The gap between the electrodes was varied between: $50\ \mu\text{m}$ (G50), $100\ \mu\text{m}$ (G100), and $500\ \mu\text{m}$ (G500). The gap width is the length of the sensing wire that will be deposited across the two electrodes. Figure 3.3b shows the mask art for making the sensing pattern, the length of the sensing wire which to be put across the electrodes was varied: $50\ \mu\text{m}$ (W50), $100\ \mu\text{m}$ (W100), and $500\ \mu\text{m}$ (W500). Figure 3.3a and Figure 3.3b are the mask for the preliminary phase experiment. Figure 3.3c displays the mask for making the electrodes; the print shows the mask pattern for making 4 pairs of the electrodes. The size of each electrode was fixed at 3 mm x 4 mm. Figure 3.3d is the mask of the sensing part. It also contains 4 masks for the 4

sensing wires. The width of the sensing wire was fixed at $100\mu\text{m}$ (W100). Figure 3.3c and Figure 3.3d is the mask art for the second experiment.

3.2.3 Silver nanoparticles sputtering

The silver nanostructured sensor was fabricated using magnetron sputtering (Univex350). Figure 3.2f, the titanium were first deposited onto the substrate as an adhesive layer with 10 nm thickness. Next to the adhesive layer, the silver nanoparticles were sputtered onto the substrate to make the electrodes (200 nm thick). The final vacuum pressure is approximately 10^{-6} mbar. The sputtering gas is an argon gas with the gas flow rate in the chamber of 20 sccm. Details of sputtering conditions are shown in the table 3.1 to table 3.3.

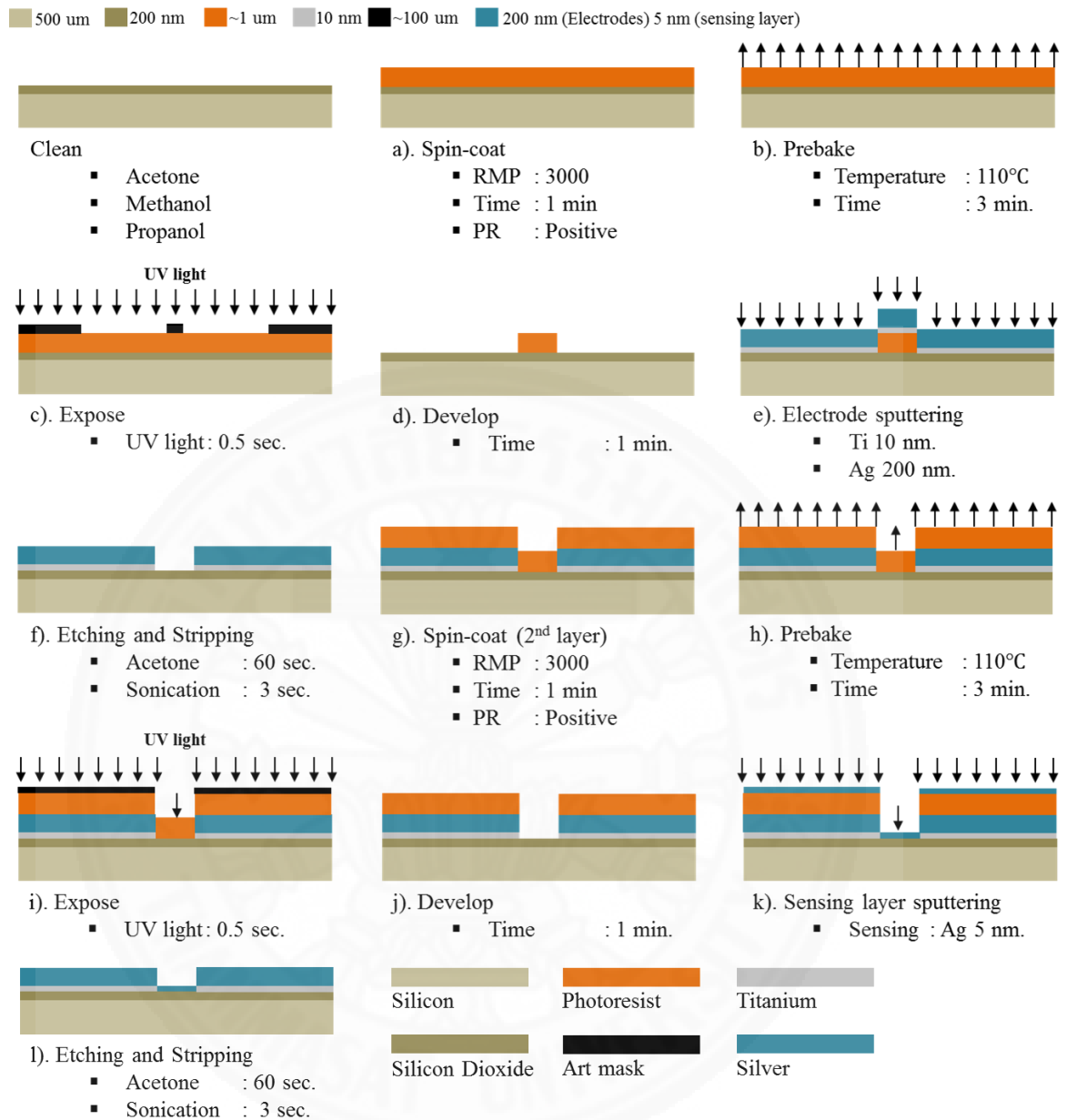


Figure 3.2 Process for fabrication of the silver nanostructured sensor

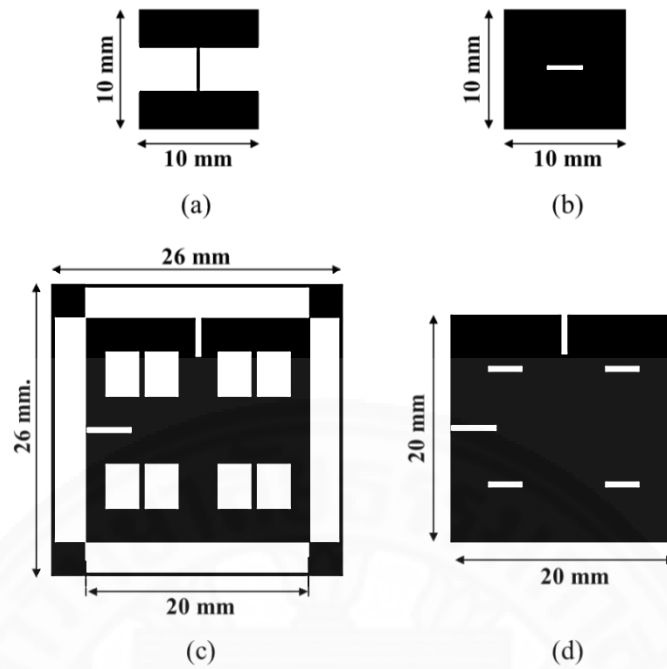


Figure 3.3 Dimensions of the masks used for making (a) the electrode pattern and (b) the sensing wire pattern used in the preliminary-phase experiment. (c) 4 pairs of electrode patterns on a single substrate, and (d) the sensing wire pattern used in the second phase experiment

Table 3.1 Sputtering conditions for the titanium adhesive layer

Adhesive layer		
Target	Titanium(Ti)	DC
Final vacuum pressure	10^{-6}	mbar
Used pressure	10^{-3}	mbar
Gas flow rate : Argon(Ar)	20	sccm
Deposition rate	0.1	Å/sec
Power set point	120	Watt
Final thickness	10	nm

Table 3.2 Sputtering conditions for the silver electrode layer

Electrodes layer		
Target	Silver(Ag)	RF
Final vacuum pressure	10^{-6}	mbar
Used pressure	10^{-2}	mbar
Gas flow rate : Argon(Ar)	20	sccm
Deposition rate	1-1.5	Å /sec
Power set point	100	Watt
Final thickness	200	nm

Table 3.3 Sputtering conditions for the sensing layer (sensing silver wire)

Sensing layer		
Target	Silver(Ag)	DC
Final vacuum pressure	10^{-6}	mbar
Used pressure	10^{-2}	mbar
Gas flow rate : Argon(Ar)	20	sccm
Deposition rate	0.4-0.7	Å /sec
Power set point	120	Watt
Final thickness	5	nm

3.2.4 Lift-off process

The silver nanoparticles deposited on the unintended part of the substrates were removed using the lift-off process as shown in Figures 3.2e-f. First, the substrates covered with silver nanoparticles were soaked in acetone for 60 sec. The substrates were then sonicated for 3 sec in order to make clear edge of the electrode. Finally, the structures were dried with gentle nitrogen gas. Figure 3.2k-l shows the lift-off process for the sensing part which follows the same steps as above.

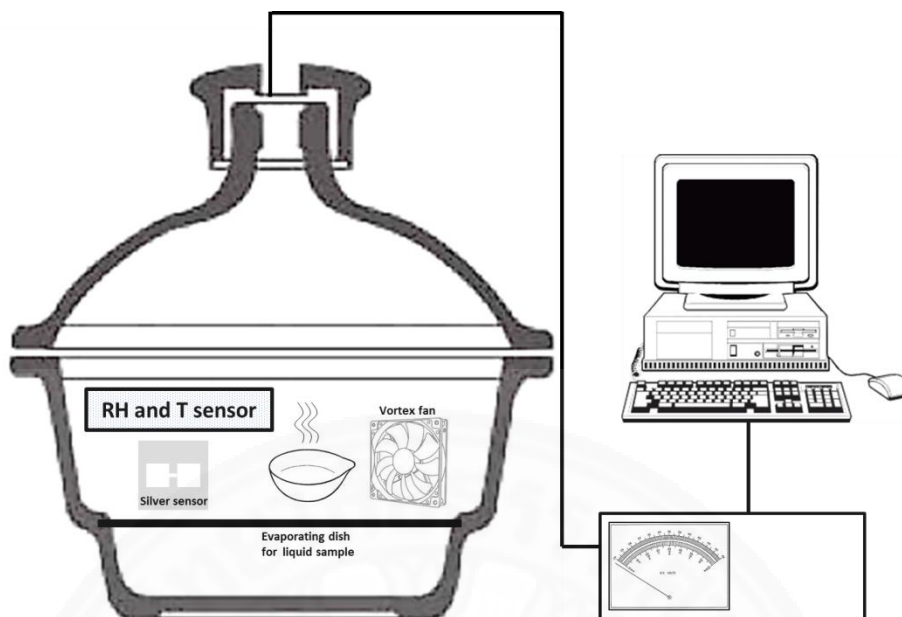


Figure 3.4 Schematic diagram of the measurement system for detecting the hydrogen sulfide and other gases.

3.2.5 Gas exposure and interface experiments

The sensor was mounted inside the desiccator which has the volume size of $23,500 \text{ cm}^3$ for ppm range experiment, and $6,900 \text{ cm}^3$ for ppb range experiment. The electrodes of the sensor were attached to the wires of the sensing meter (Fluke 45 Dual Display Multimeter). Signal changes from the sensor were sent through the wires onto a voltmeter. The voltmeter connected with a computer to collect real time sensor response data. The humidity sensor and the temperature sensor also were mounted in the measurement system. To aid gas circulation and mixing in the chamber, the vortex fan (2-inch diameter) was also mounted. Hydrogen sulfide concentration was varied in the ppb and also ppm range: 50 ppb, 100 ppb, 500 ppb, 1,000 ppb, 100 ppm, 300 ppm, and 500 ppm. The ppm-range gas was first prepared using chemical reactions between FeS and HCl producing H_2S gas as shown below. Later when the H_2S gas cylinder was acquired, simple dilution to obtain concentration in the ppb range was carried out.

3.2.5.1 Sensor exposure to hydrogen sulfide in the ppm range

According to the hydrogen sulfide concentrations, high concentration of hydrogen sulfide from 100 to 300 ppm was prepared by chemical reaction which it occurs as the equation below

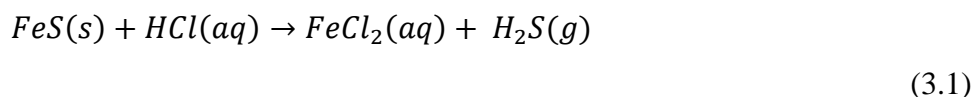


Table 3.4 Ratio between chemical precursors (*FeS and HCl (37%)*)

H ₂ S concentration (ppm)	FeS (mg)	HCl (ml)
100	2.4	1
300	7	1
500	11.5	1

The iron sulfide was put into the evaporating dish with volume following table 3.4. Then, hydrochloric acid (conc. 37%) 1 ml was injected into the evaporating dish which it contains iron sulfide before.

3.2.5.2 Sensor exposure to hydrogen sulfide in the ppb range

Hydrogen sulfide gas samples at low concentration were prepared by injecting certain volume of the 150-ppm hydrogen sulfide into the desiccator chamber filled with ordinary room air. The volume of hydrogen sulfide that was injected into desiccator depending on the concentration needed. Concentration of hydrogen sulfide was varied: 50 ppb, 100 ppb, 500 ppb, and 1,000 ppb. Table 3.5 shows volumes of hydrogen sulfide gas used for dilution to lower concentration.

Table 3.5 Dilution of the 150-ppm hydrogen sulfide gas in the 6,900 cm³ desiccator chamber

Desiccator 6.9 l	Required Concentration (ppb)	Volume injected in ml(H ₂ S @ 150 ppm)
	50	2.3
	100	4.6
	500	23
	1000	46

3.2.6 Interference experiments

To test the response of the sensor to other gases such as acetone, methanol, chloroform, dichloromethane and toluene, the liquid phase of each sample was injected into the desiccator and allowed to completely evaporate which makes the final gas concentration of 5,000 ppm. Resistant changes of the sensor were recorded real time for 10 minutes. Furthermore, the sensor was also tested for the response to water vapor in the normal air, and also tested under different relative humidity of 0%, 50%, and 70%. The relative humidity (%RH) in the lab was 65-70%, as measured by humidity sensor at room temperature (25 °C).

3.2.7 Characterization testing

Optical microscope, and field emission scanning electron microscope (FE-SEM) was used to investigate morphologies of the silver nanostructure before and after expose to H₂S gas. Energy-dispersive x-ray spectrometer (EDS) was used to observe elements after expose to H₂S gas. X-ray diffraction (XRD) further was used to investigate that the silver nanostructured sensor formed to Ag₂S after the sensor exposed to H₂S gas.

Chapter 4

Results and Discussion

4.1 Sensor fabrication results

4.1.1 Results of sensor fabrication in the preliminary phase

The preliminary experiment was intended to find suitable conditions for sensor fabrication and their initial response and stability just under ambient atmosphere. The size of the substrate in this experiment is 10 mm x 10 mm x 0.5 mm. Figure 4.1 shows the photo of the sensor fabricated. The mask pattern for this sensor was shown previously in Figure 3.3a. The resistance of this sensor can be calculated from the following equation:

$$R = \rho \frac{L}{A} \quad (4.1)$$

Where, R is resistance of the sensor, ρ is resistivity of silver in $\Omega \cdot m$, L is the length of the gap between the electrodes, and A is the cross-sectional area.

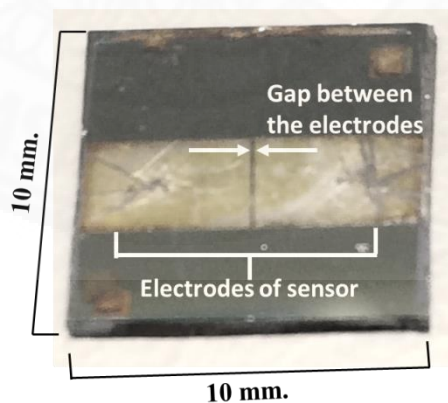


Figure 4.1 The example of sensor from the preliminary experiment. The gap between the electrodes is $100 \mu m$ (G100). The width of the sensing is $100 \mu m$ (W100). The sensor exposed to hydrogen sulfide effect on the changes of color from silver color to be yellow. For the preliminary experiment, the nanoparticles from sputtering process also appear around the side of substrate which they might connect with electrodes.

Table 4.1 Resistances of the sensors for preliminary phase from calculations and from measurements.

No.	Sensor	Resistance (Ω) (calculation)	Resistance (Ω) (Actual _{avg})
1	G50-W50-1	3.18	1.7
2	G50-W50-2		87.7
3	G50-W50-3		1,525
4	G50-W50-4		227
5	G50-W50-5		1,437
6	G100-W50-1	6.36	4.3
7	G100-W50-2		4.3
8	G100-W50-3		4.7
9	G100-W50-4		4.0
10	G100-W50-5		4.4

Table 4.1 shows the average of actual resistances of the sensors which they were measured every 3 days. The average values came from whole measurements (15 days). The results show that the sensors in this preliminary-phase experiment are not uniform with wide fluctuation in their resistance values. The sensors which are fabricated under the same condition should have the same resistance or values that are quite close to each other. The measured resistances of the sensors are not close to the expected calculated resistance, especially for the G50-W50 sensors.

Figure 4.2 shows the long term stability plots of silver nanostructured sensors of the preliminary experiment for 15 days at ambient atmosphere. The gap between the electrodes is $50 \mu m$ (G50), and the width of the sensing wire is $50 \mu m$ (W50). Over the period of 15 days, the plots of the resistance versus days of storage are quite constant for the sensors G50-W50-4 and G50-W50-5. For G50-W50-1, G50-W50-2, and G50-W50-3, the resistance versus days of storage are not constant. The resistance increased with increase in time (days) implying that they cannot use for sensors.

This fluctuation in the resistance values as well as the growth in resistance of some sensors with time of storage, especially the G50 set, are probably the result of the

strayed silver nanoparticles from the sputtering process around the electrodes. These result in the unstable resistances while measuring the resistance of the sensors.

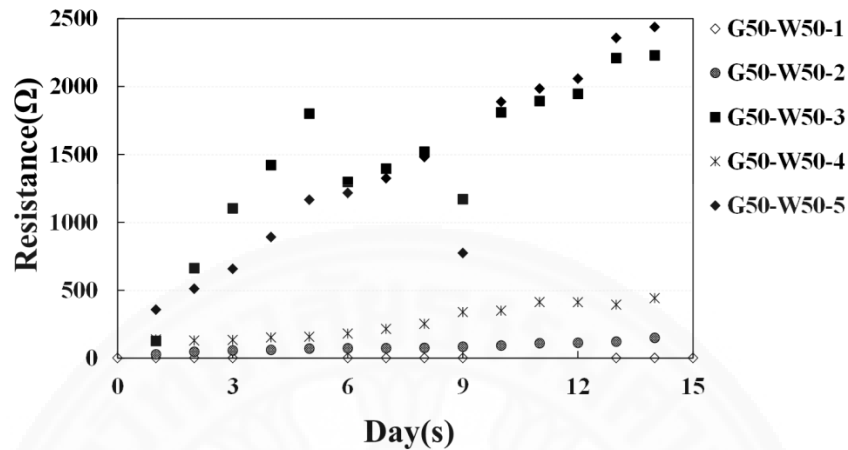


Figure 4.2 Long term stability plots of silver nanostructured sensors of preliminary experiment for 15 days at ambient atmosphere. The gap between the electrodes is $50 \mu m$ (G50), and the width of the sensing wire is $50 \mu m$ (W50).

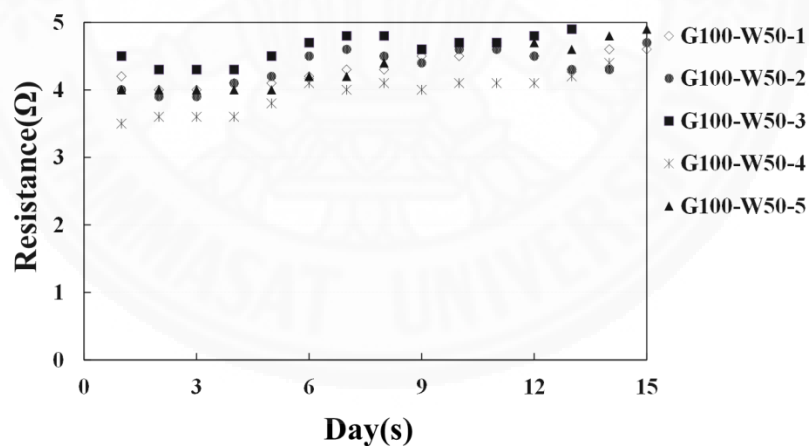


Figure 4.3 Long term stability plots of silver nanostructured sensors of preliminary experiment for 15 days at ambient atmosphere. The gap between the electrodes is $100 \mu m$ (G100), and the width of the sensing wire is $50 \mu m$ (W50).

Figure 4.3 shows long term stability plots of silver nanostructured sensors for 15 days at ambient atmosphere. The gap between the electrodes is $100 \mu m$ (G100), and the width of the sensing wire is $50 \mu m$ (W50). Over the period of 15 days, the plots of resistance

versus days of storage are rather constant therefore the ambient atmosphere does not affect the stability of sensors for the conditions of G100-W50. However, the size of the substrate was 10 mm x 10 mm x 0.5 mm which is rather large resulting in an inefficient fabrication process since the sensors has to be fabricated one by one according to the photolithography process.

4.1.2 Results of sensor fabrication in the second phase

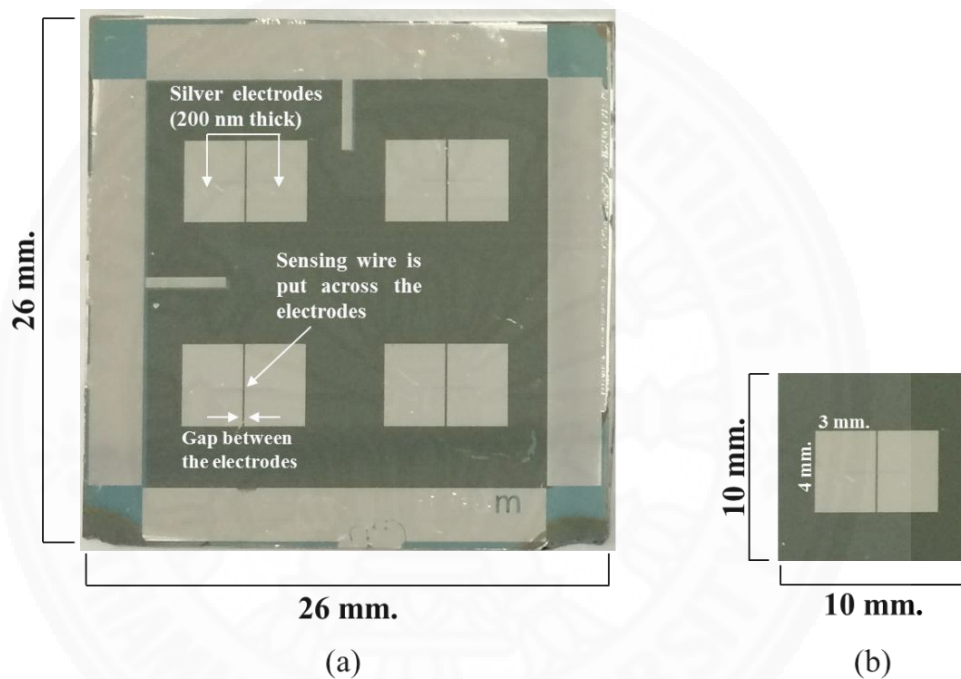


Figure 4.4 Example of sensors from the new fabrication process. The gap between the electrodes is $100\ \mu\text{m}$ (G100). The electrodes are made from the silver of 200 nm thick. The width of the sensing wire is $100\ \mu\text{m}$ (W100) which is also made from the silver of 5 nm thick). (a) The finished sensors. One substrate contains 4 sensors. (b) The substrate was cracked to separate each sensor before use in gas exposure experiment.

Based on results obtained in the preliminary experiments, we try to make the fabrication process to be more reproducible and efficient. For the new fabrication, the size of the substrate was changed to 26 mm x 26 mm x 0.5 mm. The electrodes of the sensors were reduced to 3 mm x 4 mm as represented in Figure 4.4b. One substrate now contains 4 sensors. The sensors can be separated from each other by cracking the silicon substrate. This seems to also solve the problem of nanoparticles that were sputtered

onto around the side of the substrate which probably cause an unstable resistance during the resistance measurement. The resistance of each lot (table 4.2 and table 4.3) with the same conditions is nearly similar. For example, the resistance of all sensors in the lot 1 (table 4.2) of condition G50-W100 is rather close, and the resistance of all sensors in lot 2 with the same fabrication condition (G50-W100) also have a uniform resistance. The resistance of the sensor G50-W100 for lot 1 and lot 2 are close to each other as 1.6 Ω and 1.8 Ω , respectively.

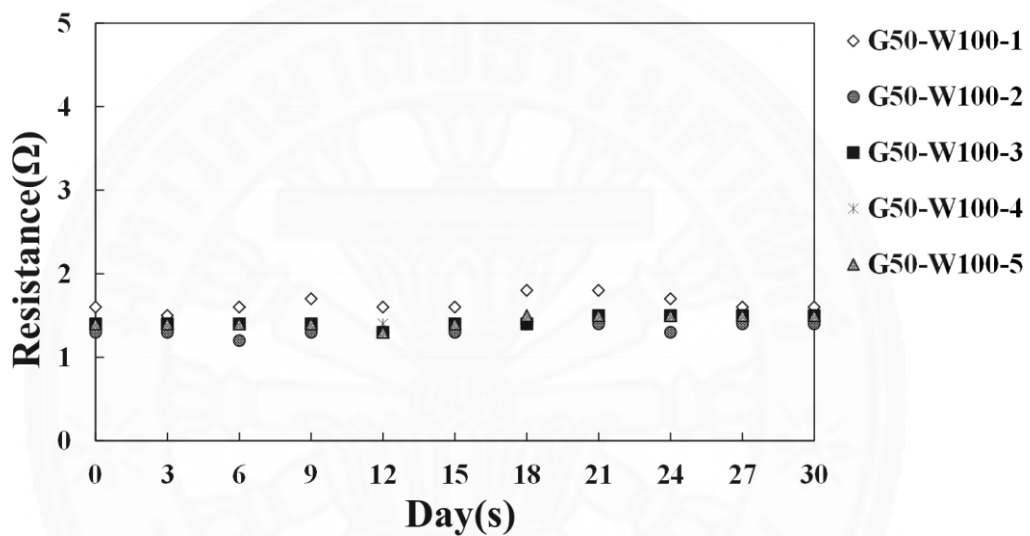


Figure 4.5 Long term stability plot of silver nanostructured sensors of the second-experiment (lot 1) for 30 days at ambient atmosphere. The gap between the electrodes is 50 μm (G50), and the width of the sensing wire was fixed at 100 μm (W100).

The actual resistances of the sensors and calculated resistances are further shown in Table 4.2 and Table 4.3. For a long term stability of the sensors over the period of 30 days, the plots of resistance versus days of storage are rather constant. Therefore the ambient atmosphere does not affect the stability of sensors as represented in Figure 4.5, Figure 4.6, Figure 4.7, Figure 4.8, Figure 4.9, and Figure 4.10.

Table 4.2 The resistances of the sensors for the second-experiment (lot 1) from calculations and measurements

No.	Sensor	Resistance (Ω) (calculation)	Resistance (Ω) (Actual _{avg})
1	G50-W100-1	1.59	1.6
2	G50-W100-2		1.3
3	G50-W100-3		1.4
4	G50-W100-4		1.4
5	G50-W100-5		1.4
6	G100-W100-1	3.18	2.6
7	G100-W100-2		2.4
8	G100-W100-3		2.3
9	G100-W100-4		3.1
10	G100-W100-5		3.8
11	G500-W100-1	15.9	17.0
12	G500-W100-2		13.7
13	G500-W100-3		12.9
14	G500-W100-4		9.7
15	G500-W100-5		7.9

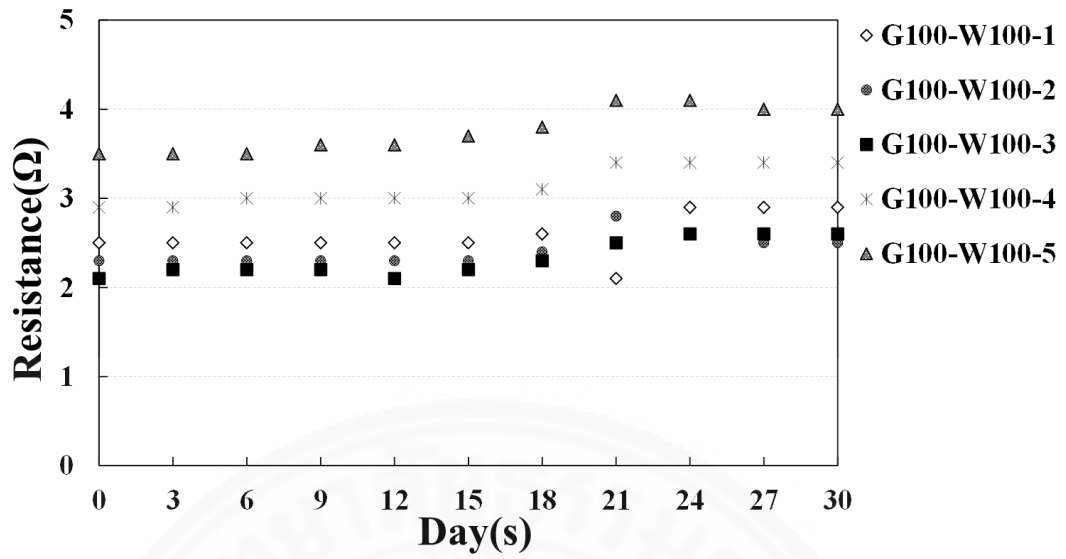


Figure 4.6 Long term stability plot of silver nanostructured sensors of second-experiment (lot 1) for 30 days at ambient atmosphere. The gap between the electrodes is $100 \mu m$ (G100), and the width of the sensing wire was fixed at $100 \mu m$ (W100).

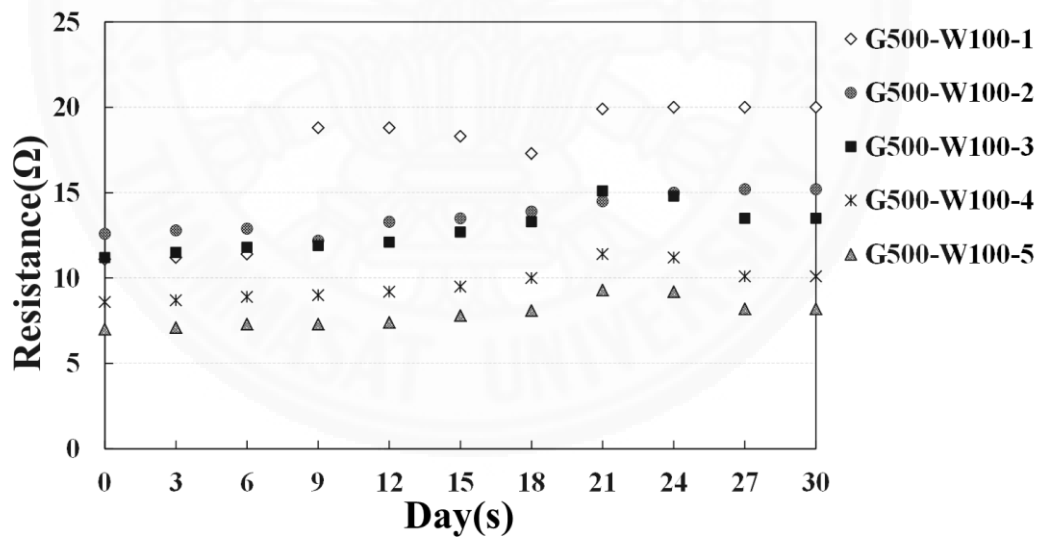


Figure 4.7 Long term stability plot of silver nanostructured sensors of second-experiment (lot 1) for 30 days at ambient atmosphere. The gap between the electrodes is $500 \mu m$ (G500), and the width of the sensing wire was fixed at $100 \mu m$ (W100).

Table 4.3 Resistances of the sensors for second-experiment (lot 2) from calculations and measurements.

No.	Sensor	Resistance (Ω) (calculation)	Resistance (Ω) (Actual _{avg})
1	G50-W100-1	1.59	1.8
2	G50-W100-2		2.0
3	G50-W100-3		2.0
4	G50-W100-4		1.8
5	G50-W100-5		2.0
6	G100-W100-1	3.18	2.2
7	G100-W100-2		2.3
8	G100-W100-3		2.3
9	G100-W100-4		2.6
10	G100-W100-5		2.6
11	G500-W100-1	15.9	6.9
12	G500-W100-2		6.0
13	G500-W100-3		8.1
14	G500-W100-4		7.1
15	G500-W100-5		7.0

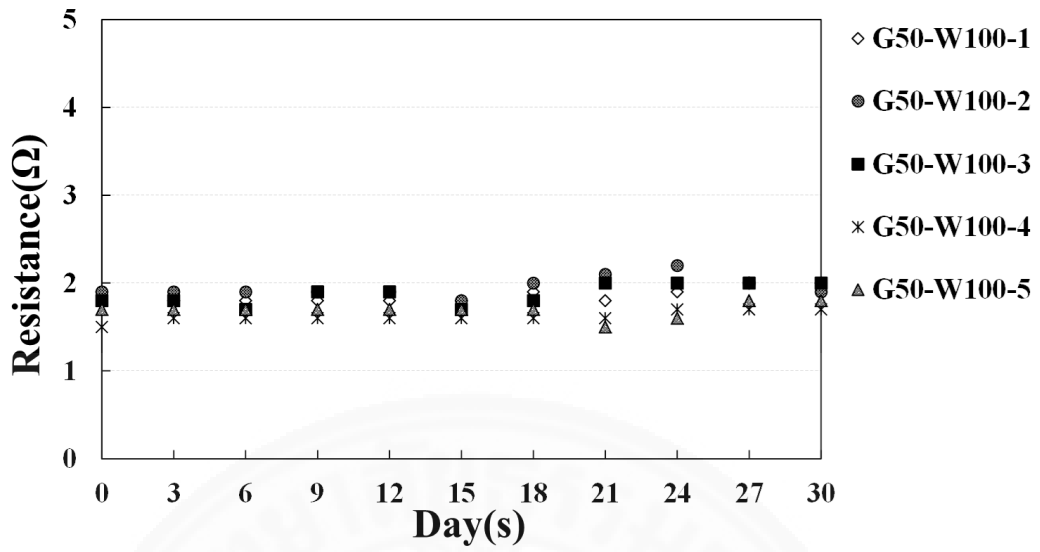


Figure 4.8 Long term stability plots of silver nanostructured sensors of second-experiment (lot 2) for 30 days at ambient atmosphere. The gap between the electrodes is $50 \mu\text{m}$ (G50), and the width of the sensing wire was fixed at $100 \mu\text{m}$ (W100).

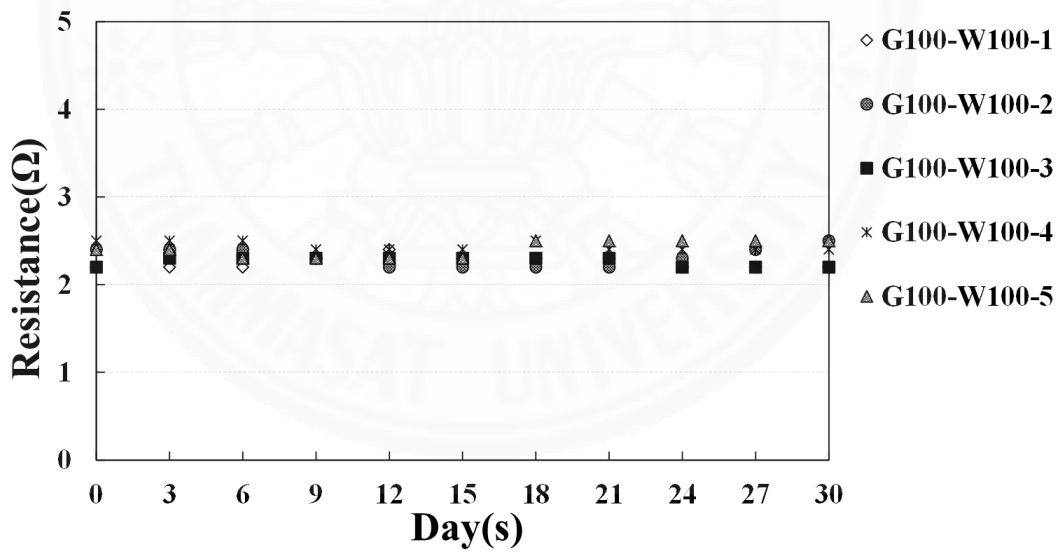


Figure 4.9 Long term stability plots of silver nanostructured sensors of second-experiment (lot 2) for 30 days at ambient atmosphere. The gap between the electrodes is $100 \mu\text{m}$ (G100), and the width of the sensing wire was fixed at $100 \mu\text{m}$ (W100).

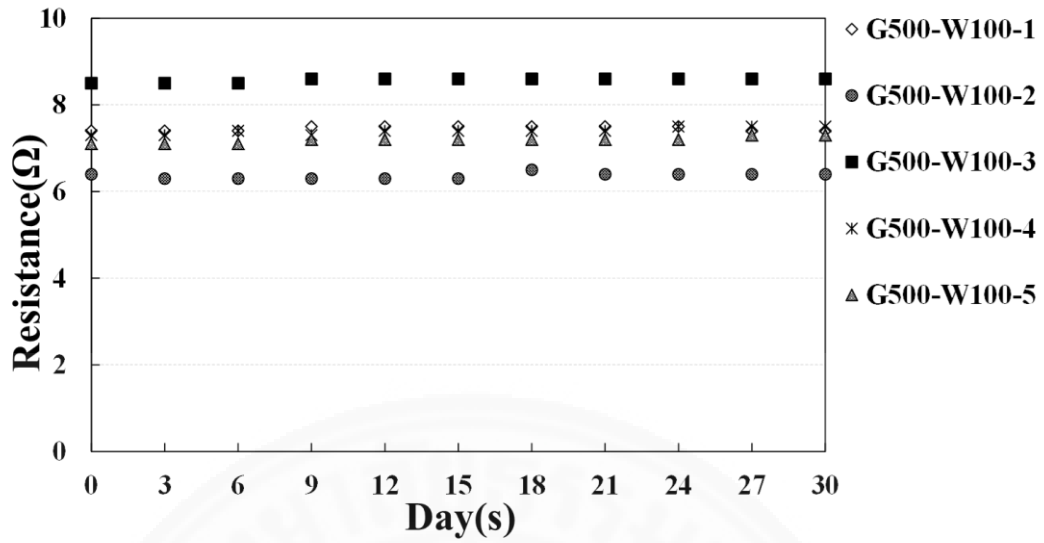


Figure 4.10 Long term stability plot of silver nanostructured sensors of second-experiment (lot 2) for 30 days at ambient atmosphere. The gap between the electrodes is 500 μm (G500), and the width of the sensing wire was fixed at 100 μm (W100).

4.2 Characterizations of the silver nanostructure sensor

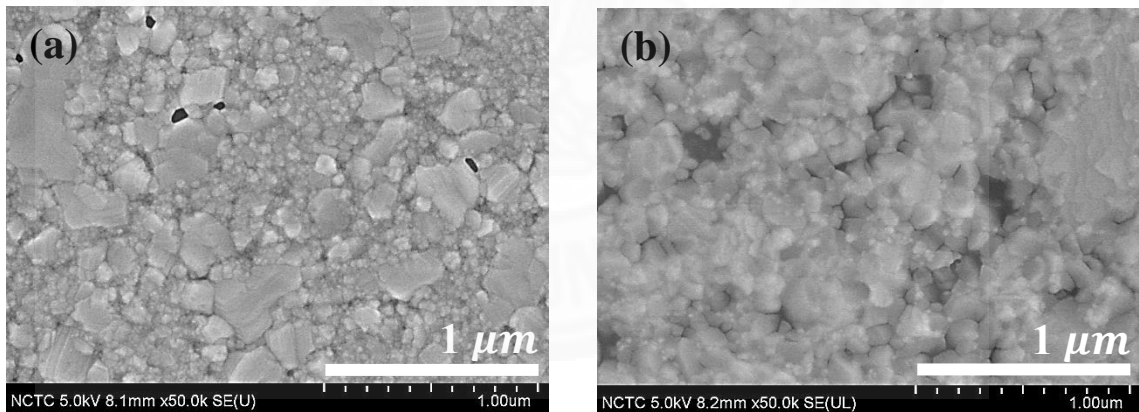


Figure 4.11 The FE-SEM images of (a) silver nanoparticles (b) silver nanoparticles after exposed to hydrogen sulfide gas for one hour at the concentration of 500 ppm. The thickness of the silver nanoparticle is five nanometers.

Figure 4.11 shows the FE-SEM images of the silver nanostructured before and after exposure to hydrogen sulfide for 5 nm thick. The images were taken at 50,000x magnification. It is found that the morphology of the silver layer that has been deposited

at the thickness of 5 nm shows clusters of silver of various grain sizes from fifty up to a few hundred nanometers. Subsequently, after the silver nanostructure was exposed to the hydrogen sulfide gas, the surface structure of the sputtered silver nanoparticles changed. The silver nanostructured seems to be more diffused forming film-like layer possibly of sulfide compound covering the previously rough grains of silver.

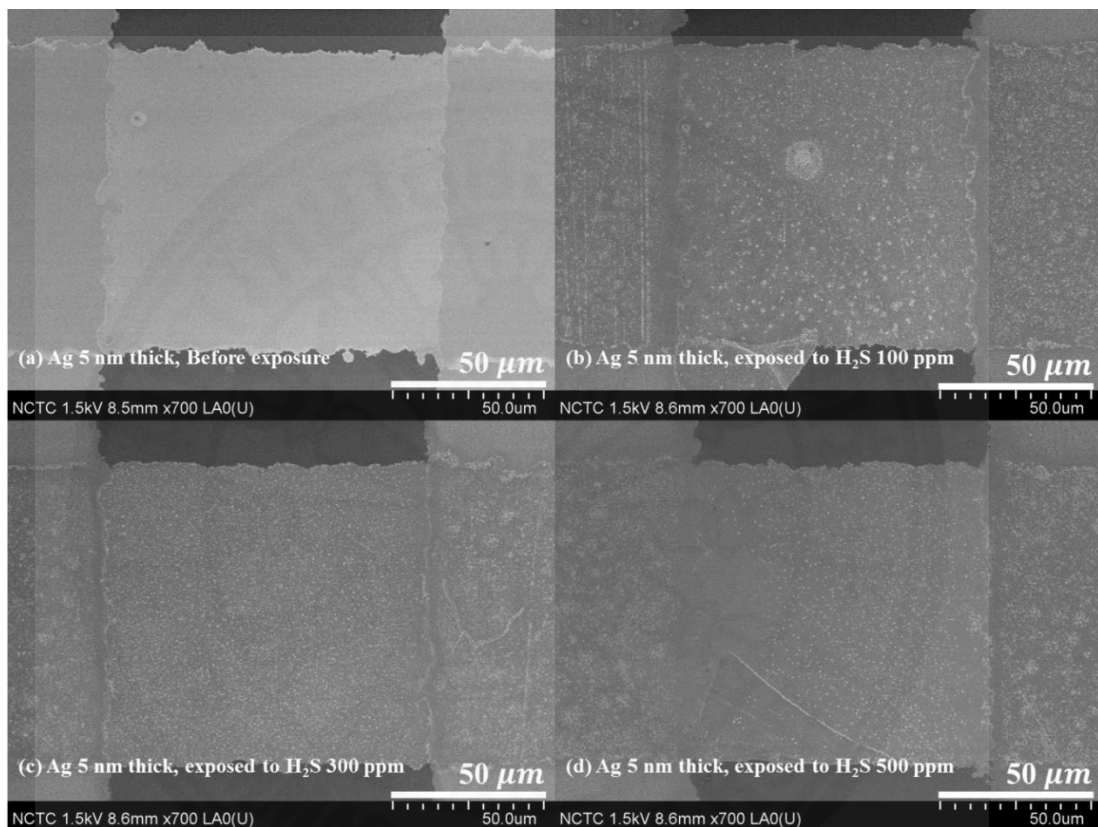


Figure 4.12 The FE-SEM images focusing on sensing part of silver sensor (a) before exposure to hydrogen sulfide gas, (b) after exposed to hydrogen sulfide at 100 ppm, (c) after exposed to hydrogen sulfide at 300 ppm, and (d) after exposed to hydrogen sulfide at 500 ppm. The images were taken at 700x magnifications.

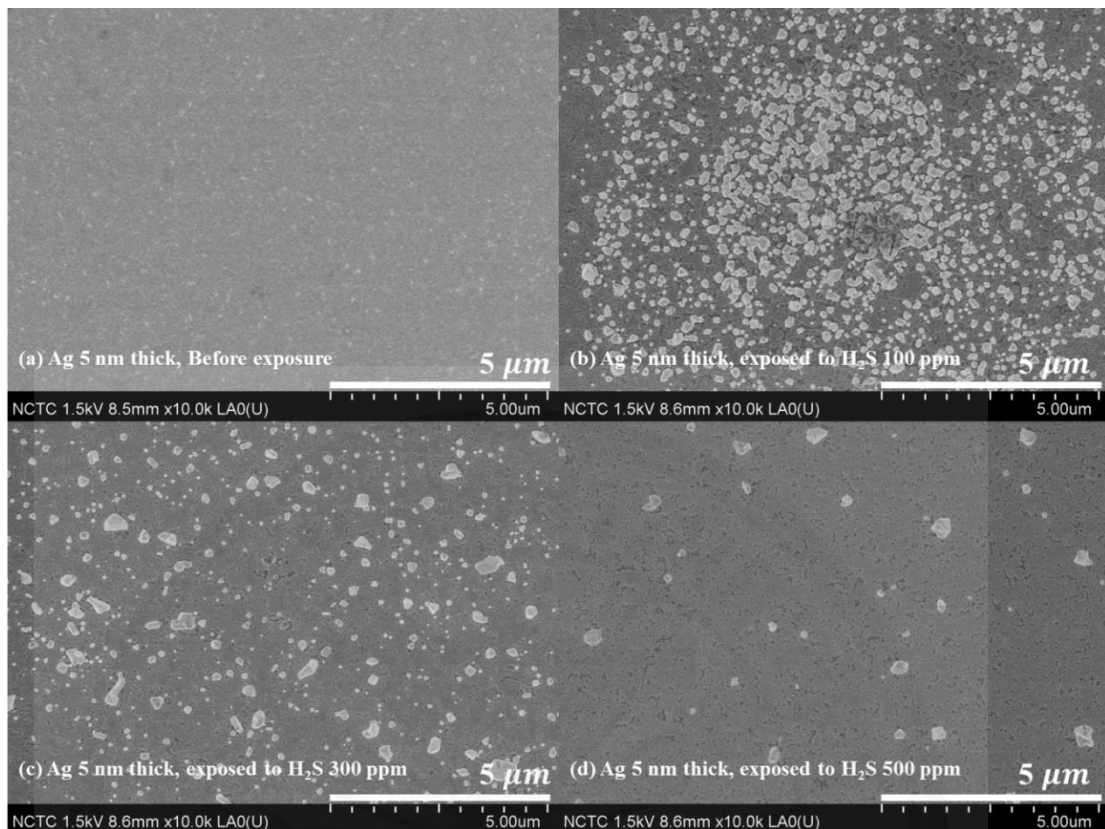


Figure 4.13 The FE-SEM images focusing on the sensing part of the silver sensor (a) before exposure to hydrogen sulfide gas, (b) after exposure to hydrogen sulfide at 100 ppm, (c) after exposure to hydrogen sulfide at 300 ppm, and (d) after exposure to hydrogen sulfide at 500 ppm. The images were taken at 10,000x magnification.

Figure 4.12 shows FE-SEM images, the sensors silver nanostructured before and after exposed to hydrogen sulfide at various concentrations. The images were taken at 700x magnifications to observe the changes of morphology with different concentration of exposure. To clearly investigate the morphology of sensors before and after exposed to hydrogen sulfide gas. The images were taken at higher magnification at 10,000x as represented in Figure 4.13. The results show that before the sensor was exposed to hydrogen sulfide gas. Nothing appears on the surface of sensing part. The morphology of the sensor before exposure was quite clear. More details are shown in Figure 4.11 at higher magnification. Figure 4.13b to Figure 4.13d, as the concentration of hydrogen sulfide is increased, the film-like area of silver nanostructure on the sensing part also increases. At the highest concentration of 500 ppm, the film-like areas appear more than other concentrations. The darker area increases with more exposure to hydrogen sulfide.

Therefore, when the silver was exposed to hydrogen sulfide. They have changes their morphology. The hydrogen sulfide gas effect on the reconstruction from rough-grain to flim-like morphology which also affects their conductivity discussed in the next section. Table 4.4 displays the EDS analysis of the silver nanoparticles 5 nm thick after exposed to hydrogen sulfide gas. The result shows that the composite contains the sulfur element. Figure 4.14 shows the XRD pattern of (a) silver nanostructured 5 nm thick prepared by magnetron sputtering. The data represents diffraction peak at $2\theta = 38.12^\circ$, 44.31° , 64.45° , and 77.41° corresponding to reflections from the planes (111), (200), (220), and (311) of pure silver, respectively. This confirmed the presence of pure silver nanocrystals on the substrate. (b) The XRD pattern of silver nanostructured 5 nm thick after exposed to hydrogen sulfide gas. It is seen that the XRD pattern exhibits the typical monoclinic (acanthite) crystal structure of silver sulfide (PDF No. 00-002-0998). The major peak reflections at $2\theta = 28.97^\circ$, 31.59° , 34.61° , 36.96° , 37.93° and 40.80° can be indexed to (111), $(11\bar{2})$, (022), (121), $(10\bar{3})$ and (031), respectively. Other peaks corresponding to (110), (200) and (220) planes are indexed with lower scattering intensity. The peaks are observed to be well matched with the standard XRD patterns of silver sulfide (PDF No. 00-002-0998).

Table 4.4 EDS result of silver nanoparticles 5 nm thick on the substrate after exposed to hydrogen sulfide gas.

Element	Weight %	Atomic %
S	4.91	14.81
Ag	95.09	85.19

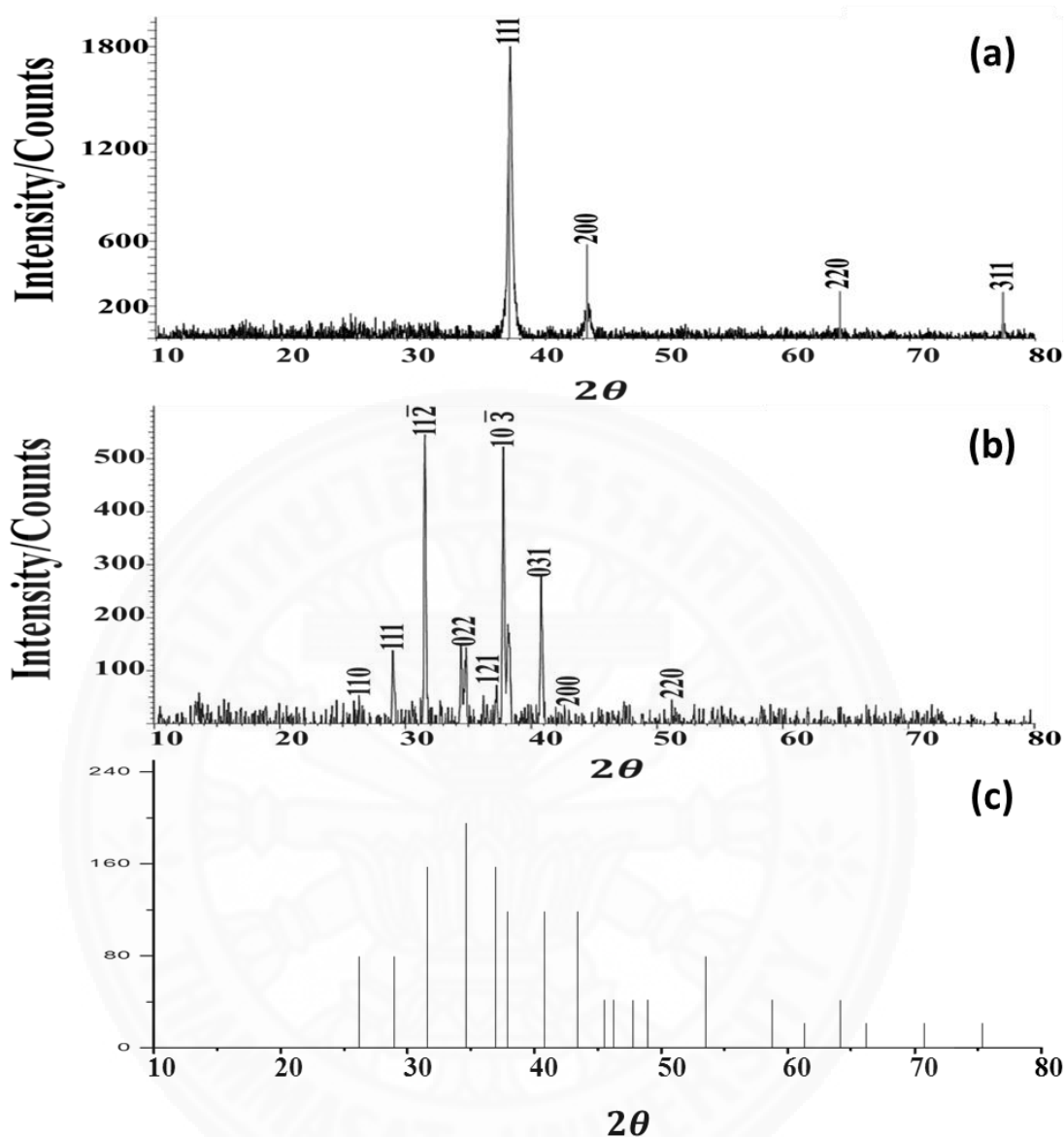


Figure 4.14 XRD spectra of (a) silver nanoparticles 5 nm thick (b) silver nanoparticles 5 nm thick after expose to hydrogen sulfide gas and (c) XRD of silver sulfide pattern (PDF 00-002-0998).

The silver nanoparticles was studied the depth morphology by using Auger electron spectroscopy (AES). Figure 4.15 shows the AES depth profiling of the fabricated silver sensing layer before and after exposure to hydrogen sulfide gas which found the sulfur on the surface down to about 5 nm depth from the top (the sputter etching rate of AES is 1 min/nm).

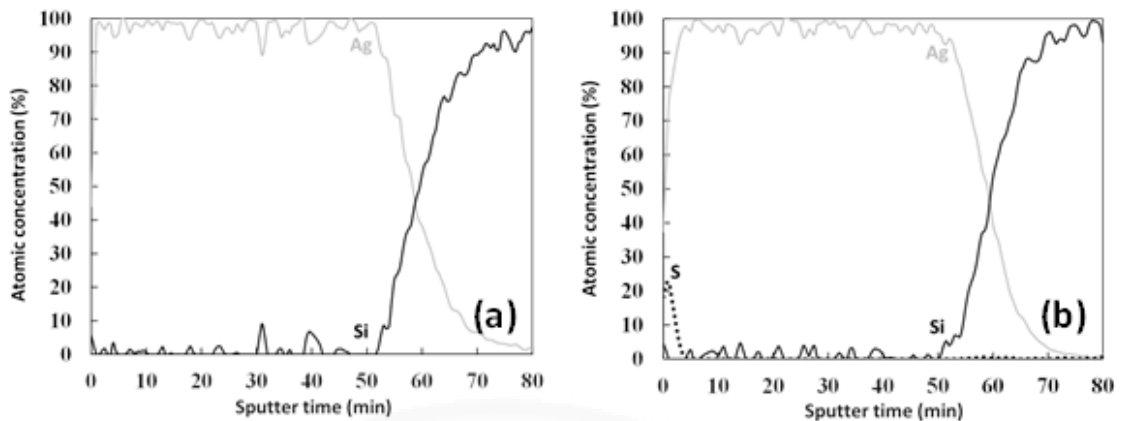


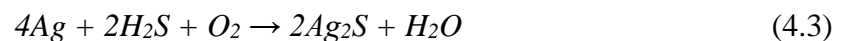
Figure 4.15 Shows results of the depth profile analysis of (a) silver 50 nm thick and (b) silver 50 nm thick after exposed to hydrogen sulfide gas (700 ppm, 1h). Sulfur is found to about 5nm depth from the Ag top surface. The thickness of Ag film as read from the AES agrees very well with the thickness read from the QCM in the sputtering machine.

4.3 Responses of Ag nanostructure sensor to hydrogen sulfide and other gases

The reaction between the hydrogen sulfide and the silver nanostructures on the surface can occur as in the equation below.



In the presence of oxygen and water vapor, the reaction might be different from the equation (4.2). Therefore reaction may be [29]:



The chemical reaction on the silver nanostructures surface when the sensor was exposed to hydrogen sulfide, silver nanoparticles forming the silver sulfide resulting in conductivity decreased. The resistances of the sensors simply expressed as $R = \rho_{eff}(L/A)$ where R is resistance of the sensor, L is the length of the gap between the electrodes, A is the cross section area of the sensing layer, and ρ_{eff} is the resistivity of

silver or silver sulfide layer in $\Omega\cdot\text{m}$. Figure 4.16 shows an equivalent circuit of silver nanoparticles 5 nm thick between the silver nanoparticles electrodes of 200 nm thickness. When the silver nanostructured sensor exposed to hydrogen sulfide, the silver nanoparticles formed silver sulfide affected the changes in resistance. Because the resistivity of silver is $1.6 \times 10^{-8} \Omega\cdot\text{m}$ but when the silver formed silver sulfide, the resistivity changed from 0.1 to $10 \Omega\cdot\text{m}$. The responses of the sensors can be given as the ratio of the resistance after silver sulfide formation (R) to the initial resistance of the pure silver film (R_0),

$$\text{Sensor response} = \frac{R_{t(\text{Ag}+\text{Ag}_2\text{S})}}{R_{0(\text{Ag})}} = \frac{R}{R_0} \quad (4.4)$$

The sensor was investigated for the effects of the gap between the electrodes and the effect of different hydrogen sulfide gas concentrations on the sensor response. For the effect of the gap length between the electrodes, the concentration of hydrogen sulfide gas was tested in the ppb and ppm range, and the sensor response recorded real time during the sensor exposure to the hydrogen sulfide gas.

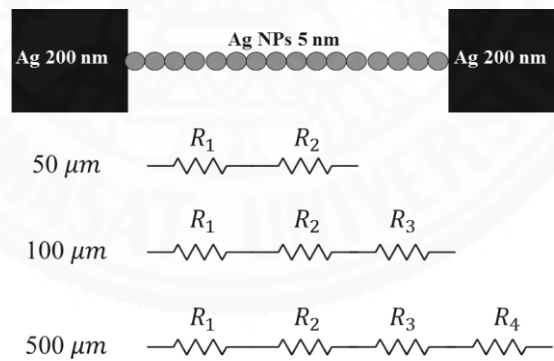


Figure 4.16 An equivalent circuit of silver nanoparticles 5 nm thick between the silver nanoparticles 200 nm thick electrodes.

4.3.1 Responses of silver nanostructures sensor to hydrogen sulfide in the ppm range

The sensor was investigated for the effect of the gap between the electrodes and the effect of different hydrogen sulfide gas concentrations on the sensor response. For the effect of the gap length between the electrodes, the concentration of hydrogen sulfide gas was kept at 300 ppm and the sensor response recorded real time during the sensor exposure to the hydrogen sulfide gas for 10 min. Figure 4.17 shows the responses of sensors with varying gap length. The response of these sensors with varying gap length are quite similar, therefore the gap length of 100 μm was selected for further investigations because of its reliable fabrication process.

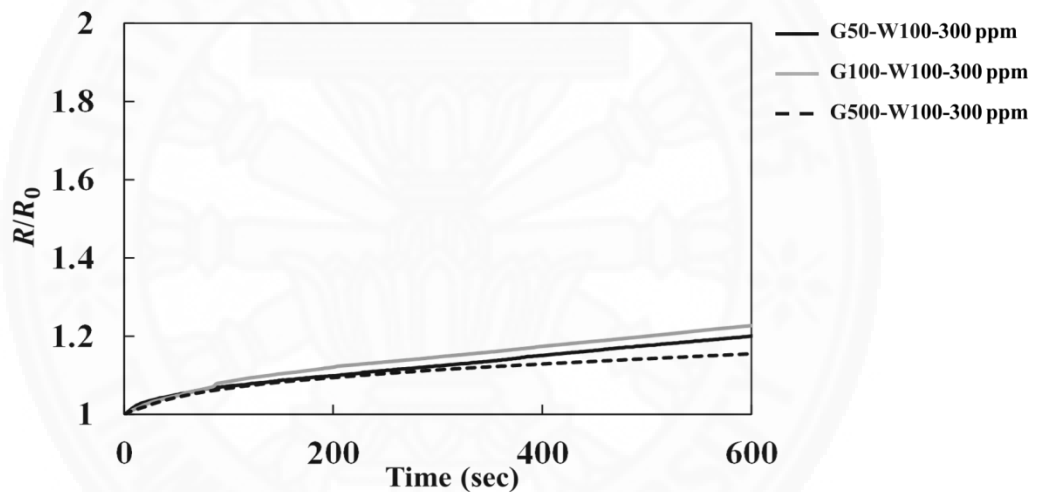


Figure 4.17 Response of sensors to hydrogen sulfide gas at 300 ppm concentration, the gap between the electrodes were varied as 50 μm (G50), 100 μm (G100), and 500 μm (G500).

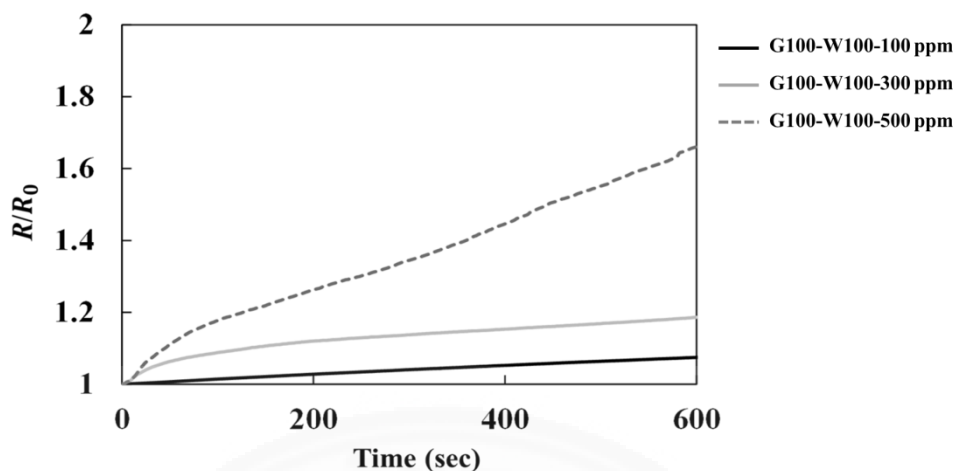


Figure 4.18 Responses of sensors (G100) to hydrogen sulfide gas at various concentrations; 100 ppm, 300 ppm, and 500 ppm.

Figure 4.18 shows the response of sensors to hydrogen sulfide gas, the gap between the electrodes was fixed at $100\ \mu\text{m}$ (G100), the concentration of hydrogen sulfide gas was varied; 100 ppm, 300 ppm and 500 ppm. The sensor was exposed to hydrogen sulfide for 10 min at ambient atmosphere. The changing of resistance ratio (response) increased with increase in concentration of hydrogen sulfide as higher hydrogen sulfide concentration can react more rapidly with the silver nanoparticles.

4.3.2 Responses of silver nanostructures sensor to hydrogen sulfide in the ppb range

For ppb range, the sensor was also investigated for the effect of the gap between the electrodes and the effect of different hydrogen sulfide gas concentrations on the sensor response. Sensors were exposed to hydrogen sulfide gas for 30 min in measurement system which it is different from the ppm experiments using only 10 min because the mechanism in ppb range needs more time to observe. The gap between the electrodes was varied: $50\ \mu\text{m}$ (G50), $100\ \mu\text{m}$ (G100), and $500\ \mu\text{m}$ (G500). Each gap was investigated the effect of different hydrogen sulfide gas concentration in ppb range. The concentration of hydrogen sulfide gas was varied: 50 ppb, 100 ppb, 500 ppb, and 1,000 ppb (1 ppm). To confirm the results of the experiment, they were repeated 3 times per one condition. Figure 4.19 to Figure 4.22 show the responses of the sensors (G50-W100) to hydrogen sulfide gas with different concentration as 50 ppb, 100 ppb, 500

ppb, and 1,000 ppb (1 ppm). The gap between the electrodes was fixed at $50\ \mu\text{m}$ (G50). The width of the sensing wire also was fixed at $100\ \mu\text{m}$ (W100).

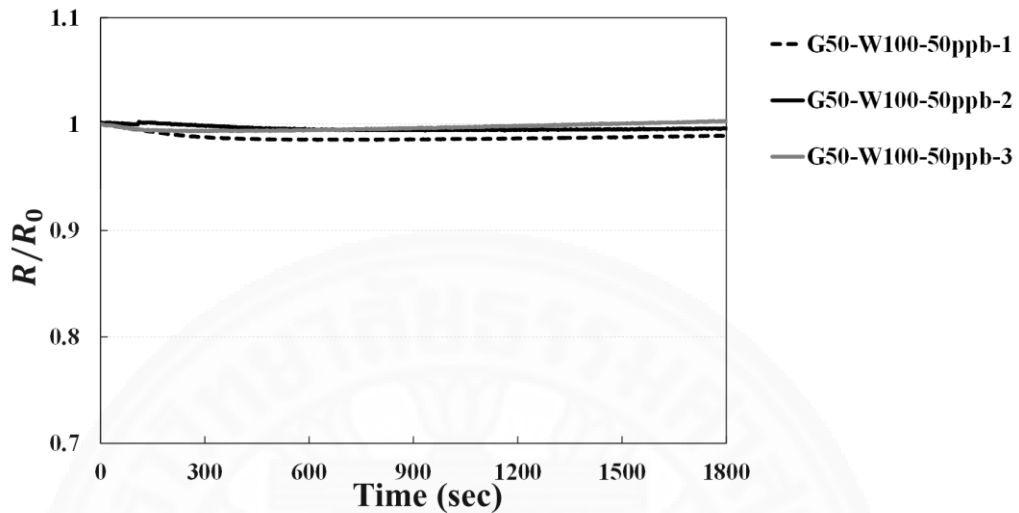


Figure 4.19 Responses of sensors (G50-W100) to hydrogen sulfide gas at 50 ppb concentration. The gap between the electrodes is $50\ \mu\text{m}$ (G50). Width of sensing wire is $100\ \mu\text{m}$ (W100).

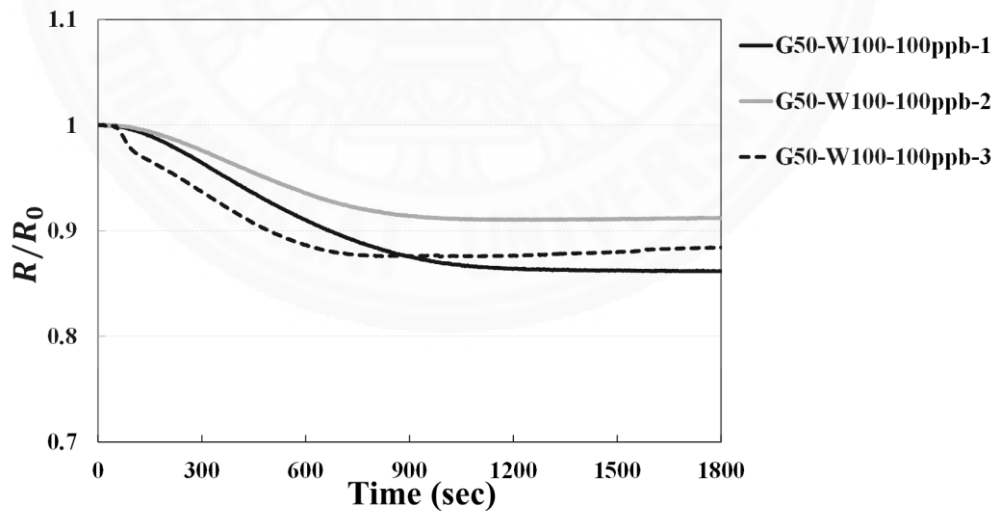


Figure 4.20 Responses of sensors (G50-W100) to hydrogen sulfide gas at 100 ppb concentration. The gap between the electrodes is $50\ \mu\text{m}$ (G50). Width of sensing wire is $100\ \mu\text{m}$ (W100).

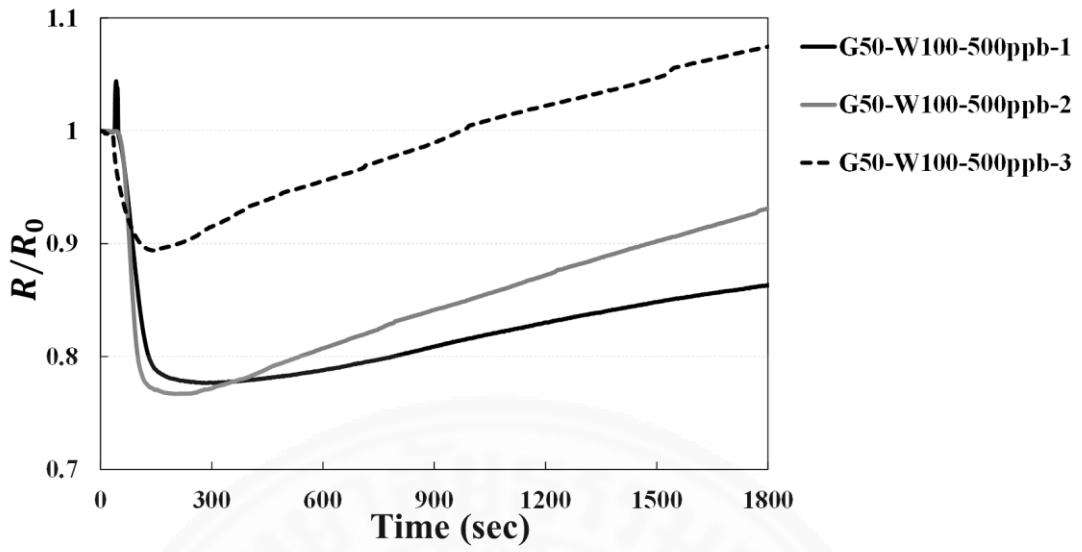


Figure 4.21 Responses of sensors (G50-W100) to hydrogen sulfide gas at 500 ppb concentration. The gap between the electrodes is $50\ \mu\text{m}$ (G50). Width of sensing wire is $100\ \mu\text{m}$ (W100).

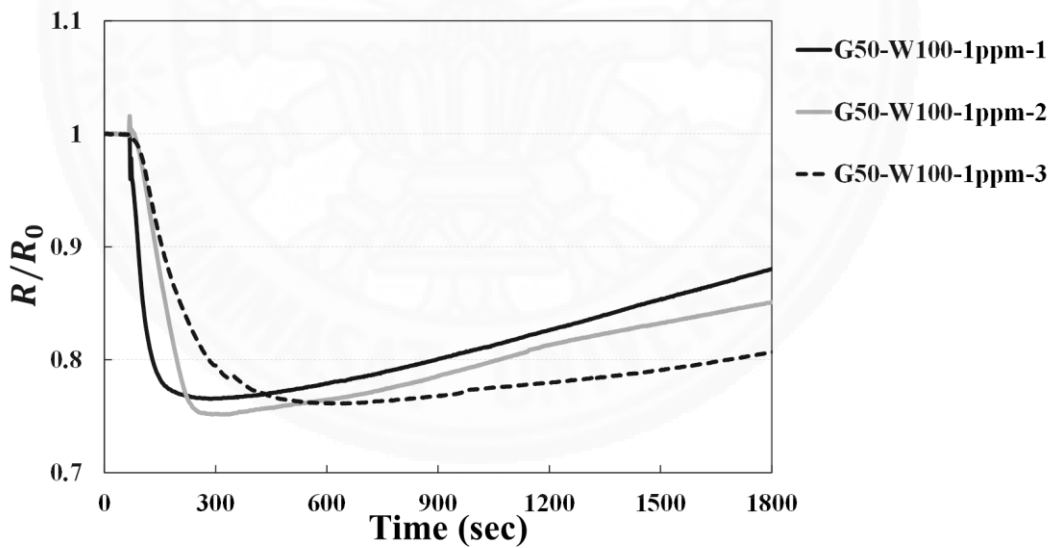


Figure 4.22 Responses of sensors (G50-W100) to hydrogen sulfide gas at 1 ppm concentration. The gap between the electrodes is $50\ \mu\text{m}$ (G50). Width of sensing wire is $100\ \mu\text{m}$ (W100).

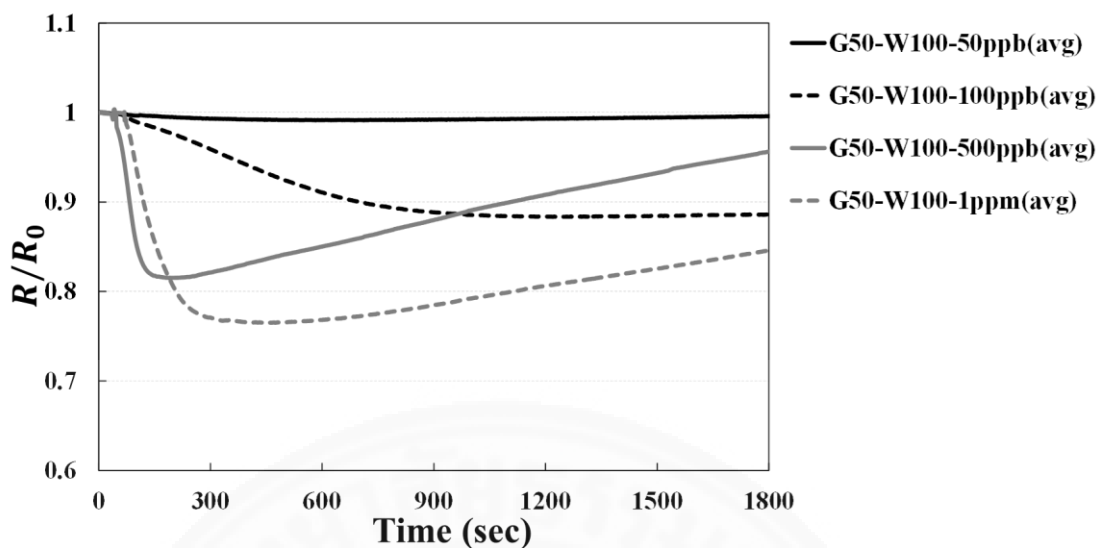
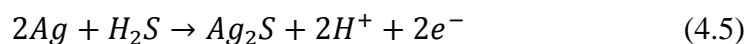


Figure 4.23 The average sensors responses of each concentration (G50-W100) to hydrogen sulfide gas at various concentrations: 50 ppb, 100 ppb, 500 ppb, and 1 ppm. The gap between the electrodes is $50 \mu\text{m}$ (G50). Width of sensing wire is $100 \mu\text{m}$ (W100).

Figure 4.23 shows the responses of the sensors G50-W100 to hydrogen sulfide gas at various concentrations: 50 ppb, 100 ppb, 500 ppb and 1,000 ppb. The response of each concentration is the average values from three repeated experiments. The results show that when the sensors were exposed to hydrogen sulfide gas, the transient resistance changed in comparison to the initial resistance. When the concentration of hydrogen sulfide gas increases, the transient conductivity of the sensors also increases. The conductivity of the sensor at 1,000 ppb or 1 ppm concentration is the fastest increase when compare with lower concentration of hydrogen sulfide gas.

According to the results, the decrease in resistance at low concentration of hydrogen sulfide in the initial exposure time period may be due to the doping effect of hydrogen sulfide to the silver metal, where free electrons where mobile ions are increased. Generally, metals have electrons on their surface. Silver metal also have electrons on their surface.

The hydrogen sulfide gas was injected into the measurement system, the conductivity of the sensor increases because of the electrons appear on the surface of the sensing more than the initial part which may occur from



According to the equation 4.5, they are two electrons per a silver sulfide as well as two hydrogen ions which can both serve as current carriers to the respective electrodes. In addition, as concentration increases, the conductivity also increases along with the amount of increased hydrogen sulfide gas because they generated the electrons more than at lower concentration. At high enough concentrations, the hydrogen and electrons may start to recombine resulting in hydrogen gas formation, depletion of silver, and increase in resistance again. In fact, when the silver formed silver sulfide, the resistance of sensor should be increase as observed in the ppm range experiments. Nevertheless, in case of ppb range contains a few of sulfur which they reacted with some of silver like silver on the surface. This effect on the conductivity of the sensor still high at the beginning because the electrons can move without barriers. However, as time increase, the resistances of the sensors slightly increase because silver sensing formed silver sulfide. The amount of silvers decreases which decreases the flow of the electrons. Figure 4.24 to 4.27 show the responses of the sensor to hydrogen sulfide gas with different concentration as 50 ppb, 100 ppb, 500 ppb, and 1,000ppb (1 ppm). The gap between the electrodes was fixed at 100 μm (G100). The width of the sensing wire also was fixed at 100 μm (W100). There are three experiments of each concentration: G100-W100-(concentration in ppb range)-1, G100-W100-(concentration in ppb range)-2, and G100-W100-(concentration in ppb range)-3.

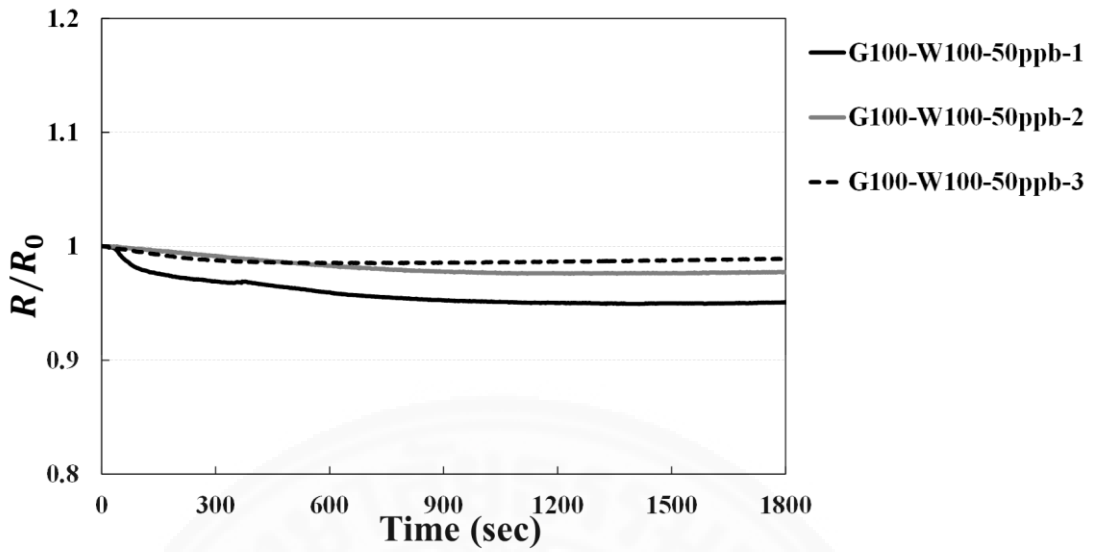


Figure 4.24 Responses of sensors (G100-W100) to hydrogen sulfide gas at 50 ppb concentration. The gap between the electrodes is 100 μm (G100). Width of sensing wire is 100 μm (W100).

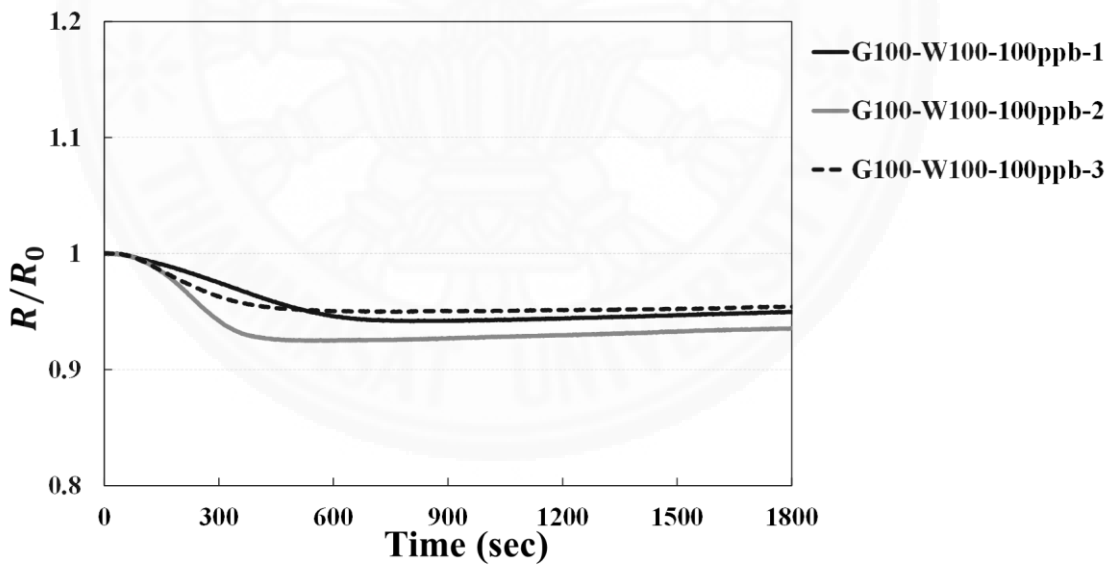


Figure 4.25 Responses of sensors (G100-W100) to hydrogen sulfide gas at 100 ppb concentration. The gap between the electrodes is 100 μm (G100). Width of sensing wire is 100 μm (W100).

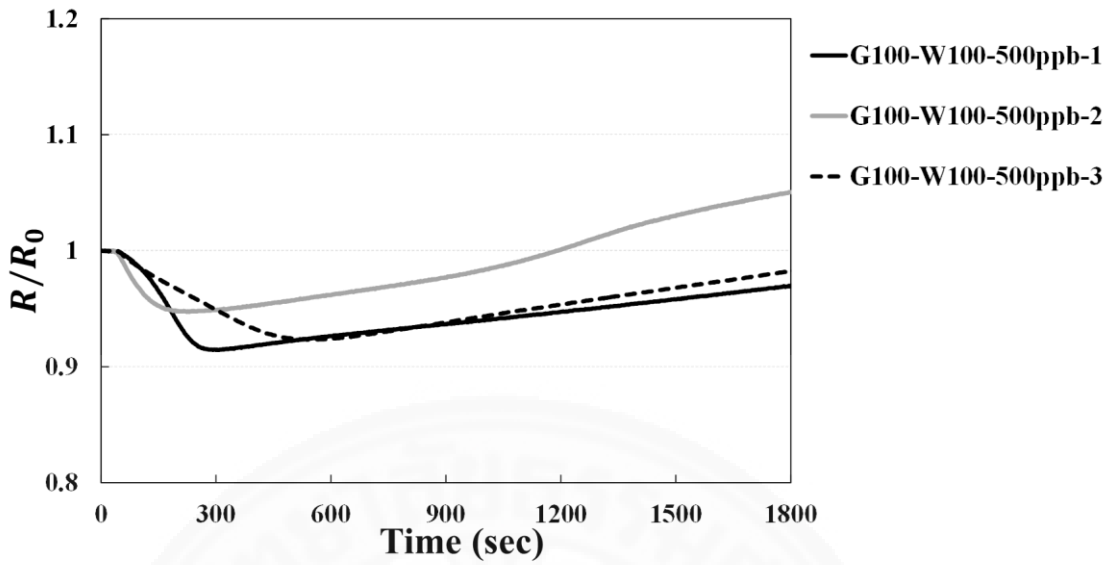


Figure 4.26 Responses of sensors (G100-W100) to hydrogen sulfide gas at 500 ppb concentration. The gap between the electrodes is $100 \mu m$ (G100). Width of sensing wire is $100 \mu m$ (W100).

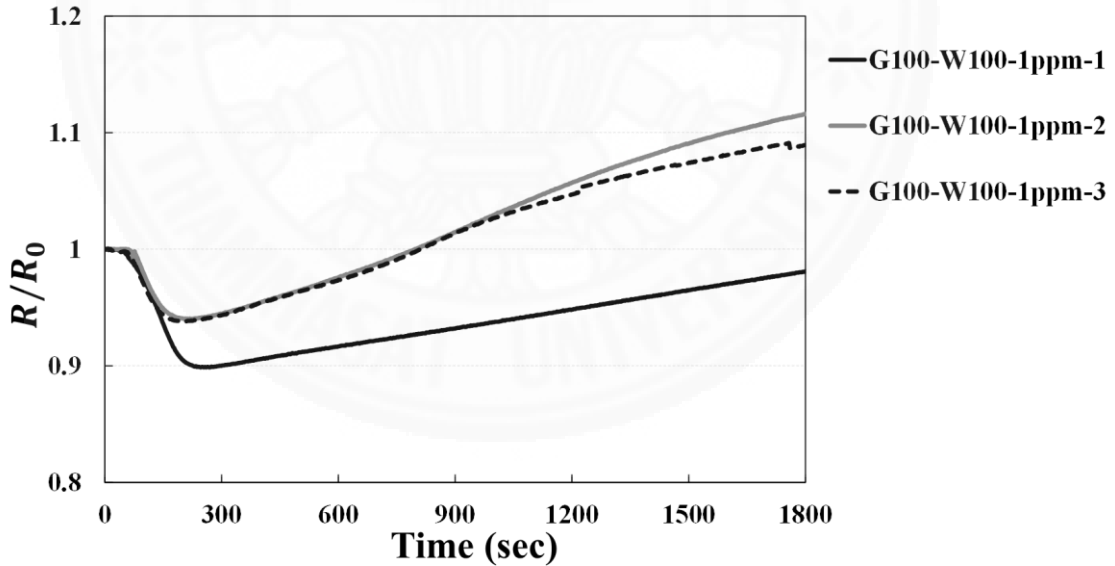


Figure 4.27 Responses of sensors (G100-W100) to hydrogen sulfide gas at 1 ppm concentration. The gap between the electrodes is $100 \mu m$ (G100). Width of sensing wire is $100 \mu m$ (W100).

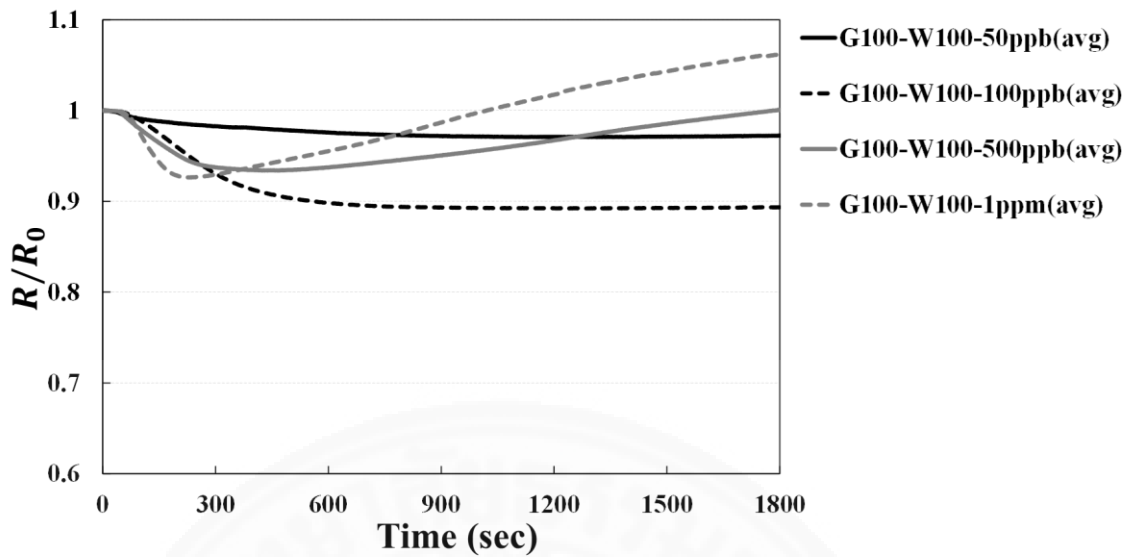


Figure 4.28 The average sensors responses of each concentration (G100-W100) to hydrogen sulfide gas at various concentrations: 50 ppb, 100 ppb, 500 ppb, and 1 ppm. The gap between the electrodes is $100\ \mu\text{m}$ (G100). Width of sensing wire is $100\ \mu\text{m}$ (W100).

Figure 4.28 shows the responses of the sensors G100-W100 to hydrogen sulfide gas at various concentrations: 50 ppb, 100 ppb, 500 ppb and 1,000 ppb (1 ppm). The response of each concentration is the average values from three repeated experiments. The results show that when the sensors were exposed to hydrogen sulfide gas, the transient resistance changed in comparison to the initial resistance. When the concentration of hydrogen sulfide gas increases, the transient conductivity of the sensors also increases. For the sensors G100-W100 have same mechanism as G50-W100 but the responses of G100-W100 have a different intensity response from G50-W100. Figure 4.29 to 4.32 show the responses of the sensor to hydrogen sulfide gas with different concentration as 50 ppb, 100 ppb, 500 ppb, and 1,000 ppb (1 ppm). The gap between the electrodes was fixed at $500\ \mu\text{m}$ (G500). The width of the sensing wire also was fixed at $100\ \mu\text{m}$ (W100). They are three experiments of each concentration: G500-W100-(concentration in ppb range)-1, G500-W100-(concentration in ppb range)-2, and G500-W100-(concentration in ppb range)-3.

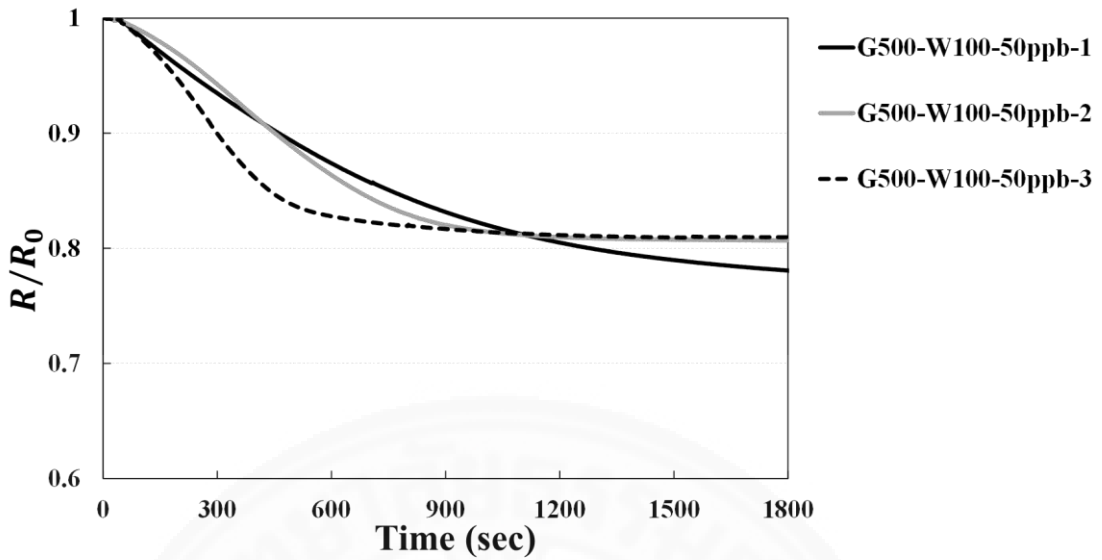


Figure 4.29 Responses of sensors (G500-W100) to hydrogen sulfide gas at 50 ppb concentration. The gap between the electrodes is 500 μm (G500). Width of sensing wire is 100 μm (W100).

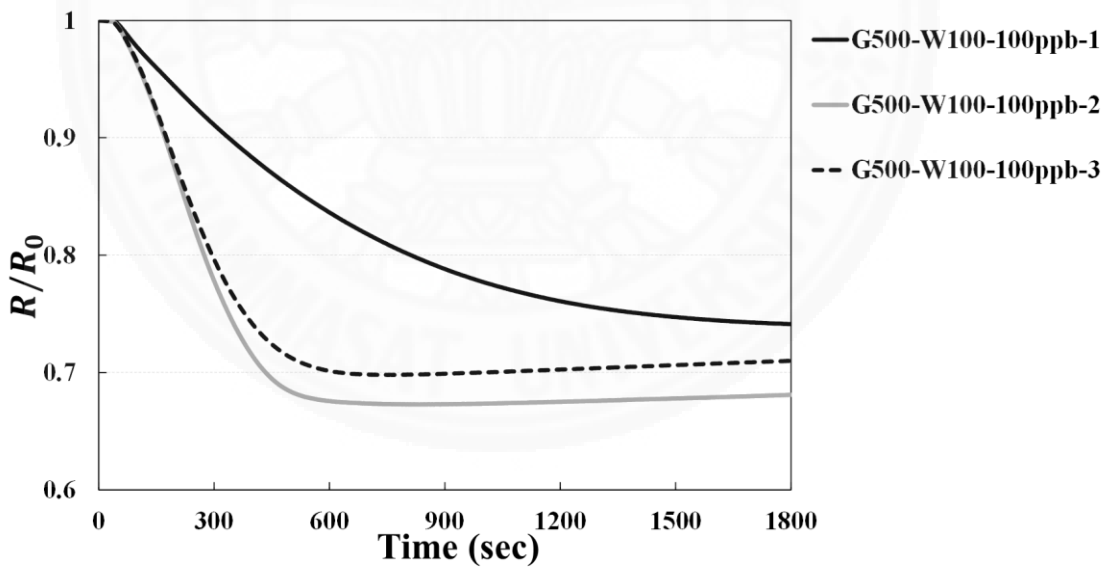


Figure 4.30 Responses of sensors (G500-W100) to hydrogen sulfide gas at 100 ppb concentration. The gap between the electrodes is 500 μm (G500). Width of sensing wire is 100 μm (W100).

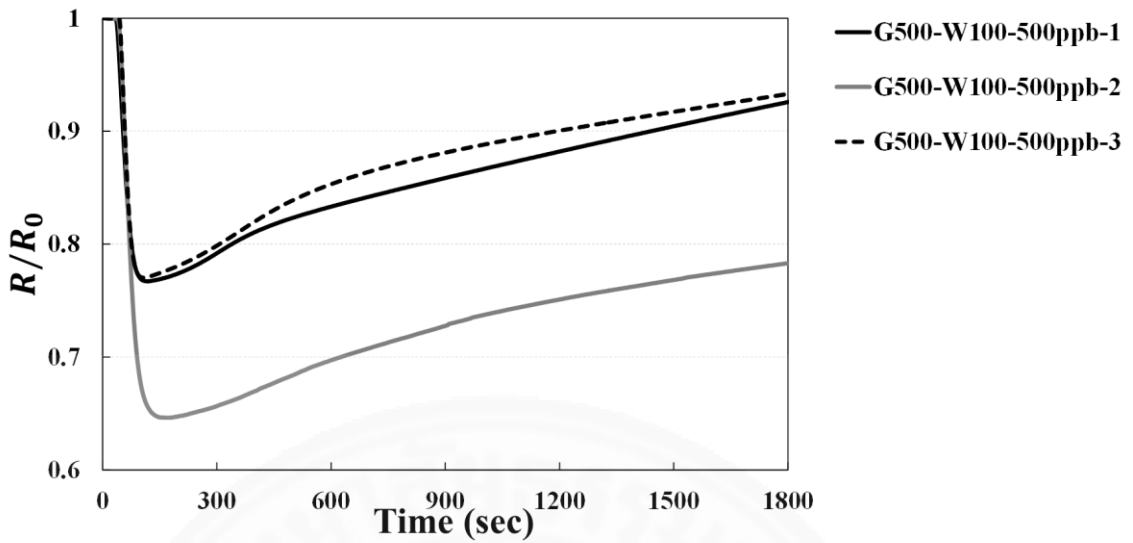


Figure 4.31 Responses of sensors (G500-W100) to hydrogen sulfide gas at 500 ppb concentration. The gap between the electrodes is $500 \mu m$ (G500). Width of sensing wire is $100 \mu m$ (W100).

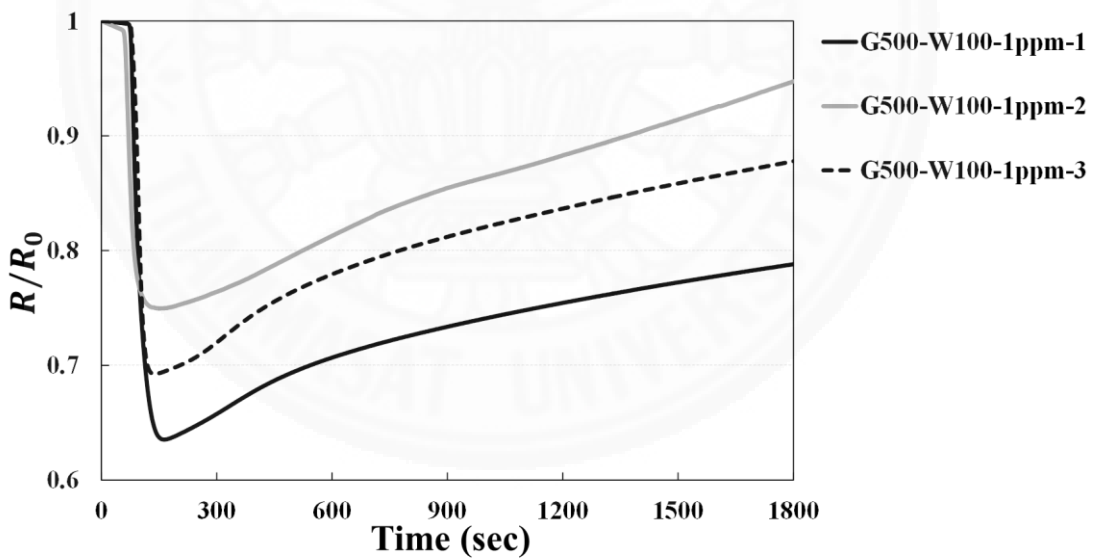


Figure 4.32 Responses of sensors (G500-W100) to hydrogen sulfide gas at 1 ppm concentration. The gap between the electrodes is $500 \mu m$ (G500). Width of sensing wire is $100 \mu m$ (W100).

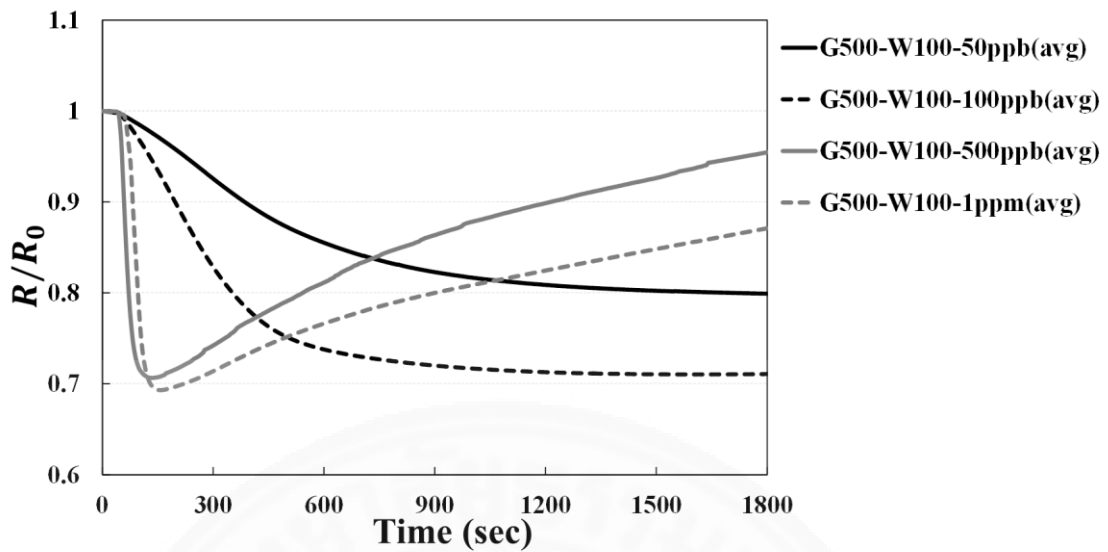


Figure 4.33 The average sensors responses of each concentration (G500-W100) to hydrogen sulfide gas at various concentrations: 50 ppb, 100 ppb, 500 ppb, and 1 ppm. The gap between the electrodes is $100 \mu m$ (G500). Width of sensing wire is $100 \mu m$ (W100).

Figure 4.33 shows the responses of the sensors G500-W100 to hydrogen sulfide gas at various concentrations: 50 ppb, 100 ppb, 500 ppb and 1,000 ppb (1 ppm). The response of each concentration is the average values from three repeated experiments. The results show that when the sensors were exposed to hydrogen sulfide gas, the transient resistance changed in comparison to the initial resistance. When the concentration of hydrogen sulfide gas increases, the transient conductivity of the sensors also increases. For the sensors G500-W100, they rapidly react with hydrogen sulfide better than G50-W100, and G100-W100 when compared the intensity of the responses. To investigate the effect of the gap between the electrodes, the sensors with various gaps between the electrodes were exposed to hydrogen sulfide gas at the same concentration as represented in figure 4.34 to 4.37.

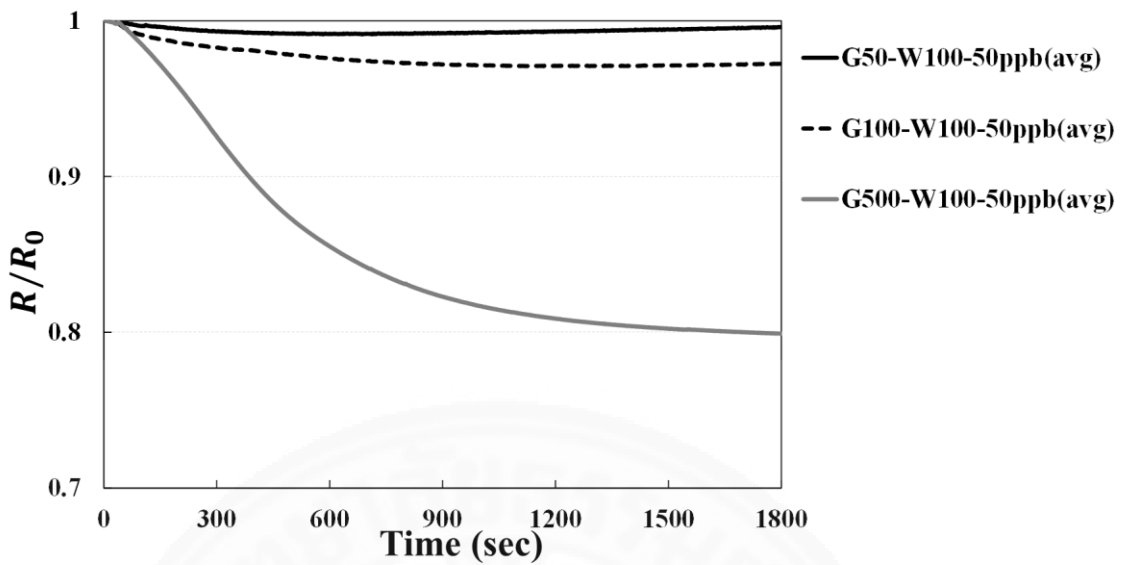


Figure 4.34 The average sensors responses to hydrogen sulfide gas at 50 ppb concentrations. The gaps between the electrodes were varied: 50 μm (G50), 100 μm (G100), and 500 μm (G500). Width of sensing wire is 100 μm (W100).

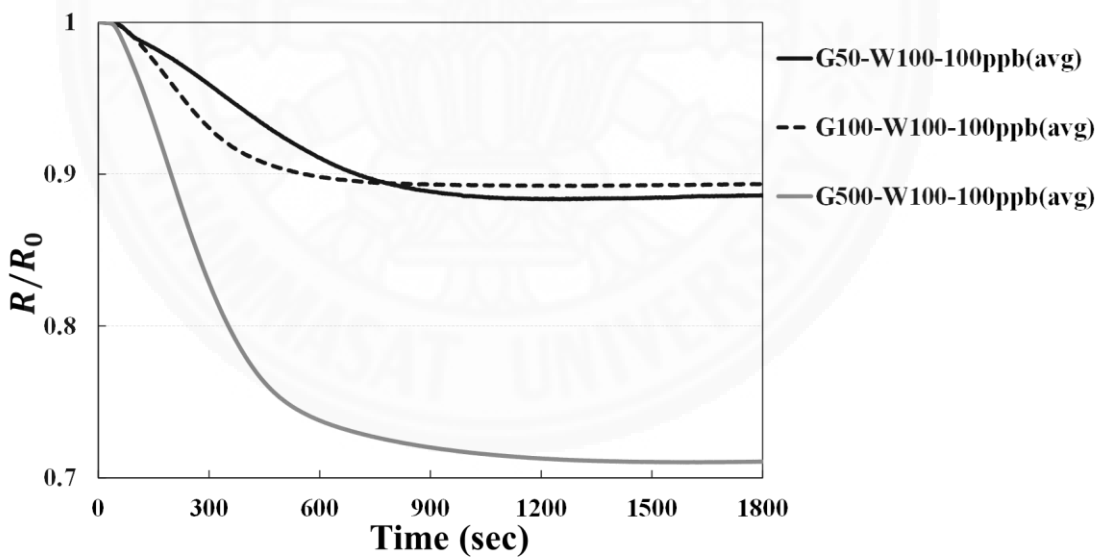


Figure 4.35 The average sensors responses to hydrogen sulfide gas at 100 ppb concentrations. The gaps between the electrodes were varied: 50 μm (G50), 100 μm (G100), and 500 μm (G500). Width of sensing wire is 100 μm (W100).

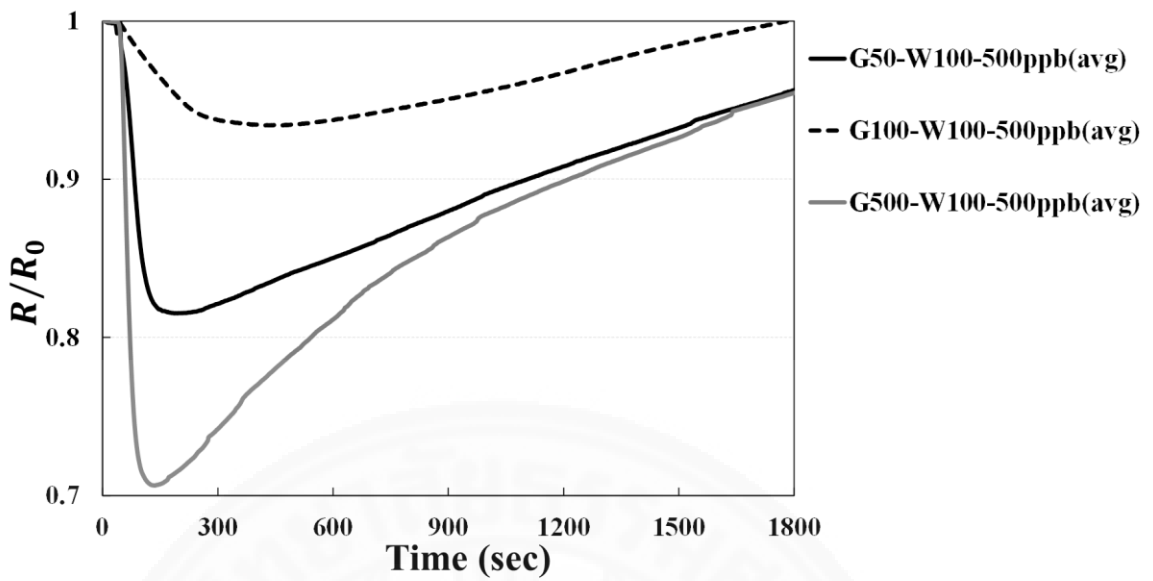


Figure 4.36 The average sensors responses to hydrogen sulfide gas at 500 ppb concentrations. The gaps between the electrodes were varied: 50 μm (G50), 100 μm (G100), and 500 μm (G500). Width of sensing wire is 100 μm (W100).

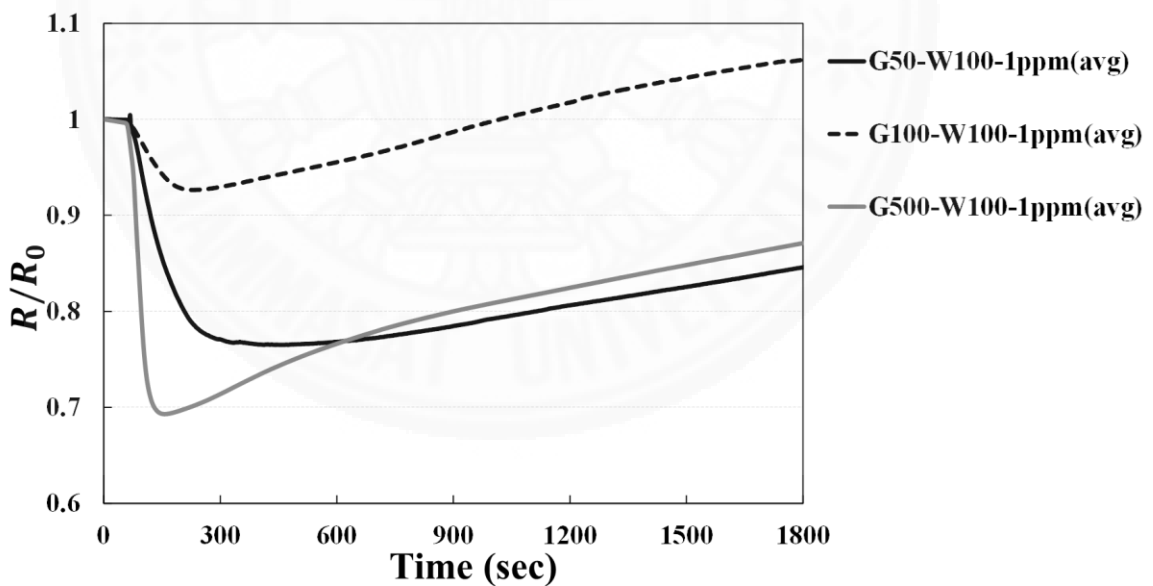


Figure 4.37 The average sensors responses to hydrogen sulfide gas at 1 ppm concentrations. The gaps between the electrodes were varied: 50 μm (G50), 100 μm (G100), and 500 μm (G500). Width of sensing wire is 100 μm (W100).

According to the results (figure 4.34 to 4.37), the G500-W100 sensor easier responds to hydrogen sulfide gas than the G50-W100 and G100-W100 for all concentrations in the ppb range, especially at 50 ppb. Because the sensing of sensor G500-W100 contains silver nanoparticles more than G50-W100 and G100-W100 which cause the increased in probability for the silver to react with the hydrogen sulfide gas.

4.3.3 Investigation on interference from water vapor (air humidity), and other gases

To test the response of the sensors for the other gases such as acetone, methanol, chloroform, dichloromethane and toluene, the gases were injected into the desiccator with the final gas concentration in the chamber of 5,000 ppm. Furthermore, the responses of sensors to humidity were also observed. The change in resistance of the sensor was recorded real time for 30 min.

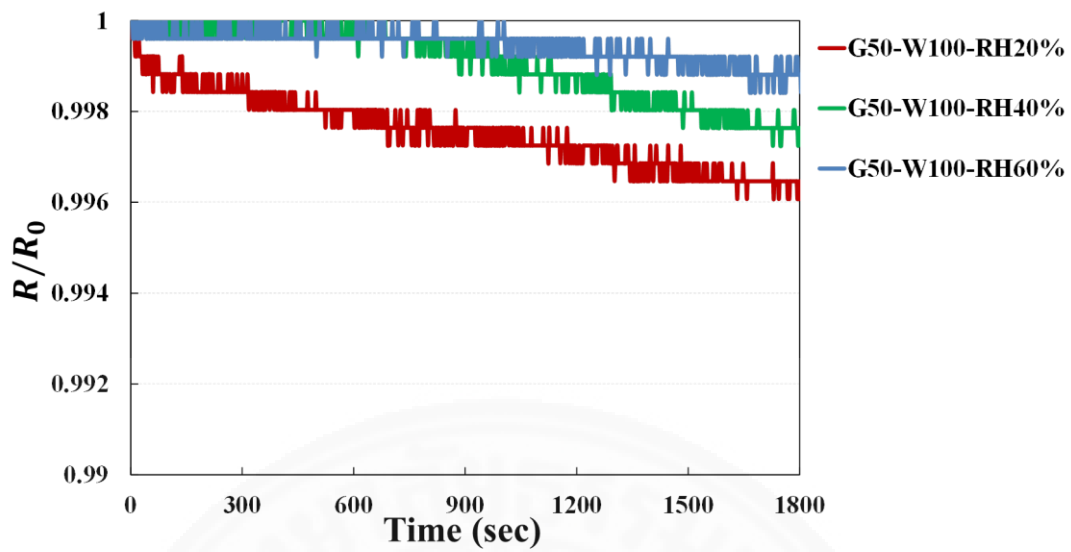


Figure 4.38 The responses of sensors to humidity. The humidity was varied: 20%, 40%, and 60%. The gap between the electrodes is $50\ \mu\text{m}$ (G50). The sensing wire is $100\ \mu\text{m}$ (W100).

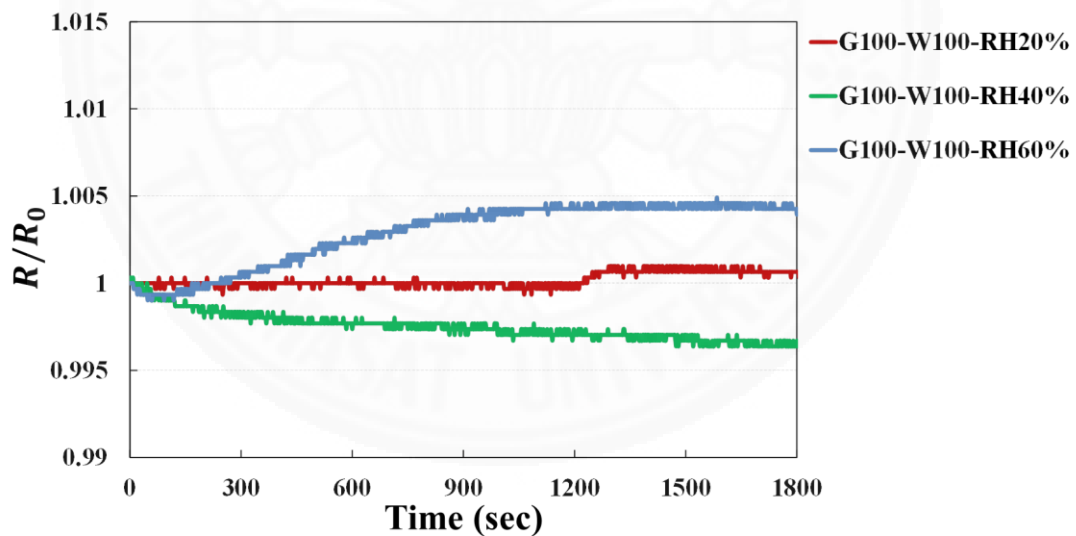


Figure 4.39 The responses of sensors to humidity. The humidity was varied: 20%, 40%, and 60%. The gap between the electrodes is $100\ \mu\text{m}$ (G100). The sensing wire is $100\ \mu\text{m}$ (W100).

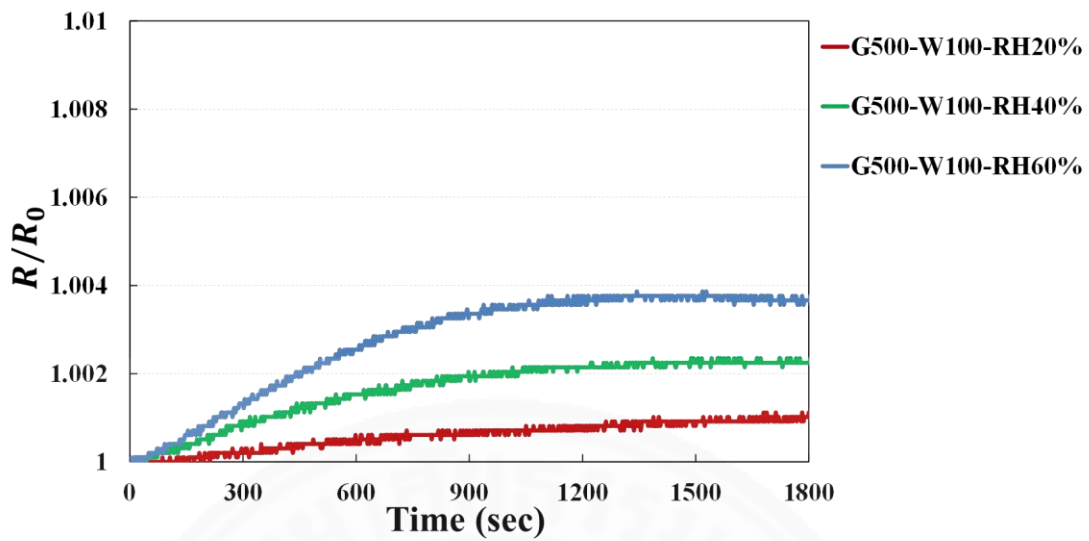


Figure 4.40 The responses of sensors to humidity. The humidity was varied: 20%, 40%, and 60%. The gap between the electrodes is $500\ \mu\text{m}$ (G500). The sensing wire is $100\ \mu\text{m}$ (W100).

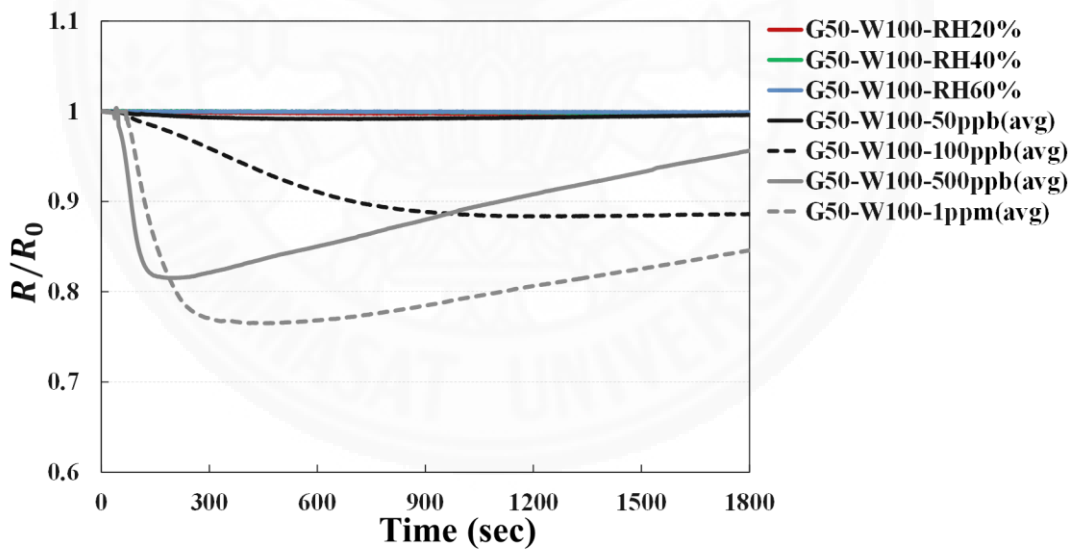


Figure 4.41 The responses of sensors to hydrogen sulfide compare to humidity. The humidity was varied: 20%, 40%, and 60%. Hydrogen sulfide gas was varied: 50 ppb, 100 ppb, 500 ppb, and 1 ppm. The gap between the electrodes is $50\ \mu\text{m}$ (G50). The sensing wire is $100\ \mu\text{m}$ (W100).

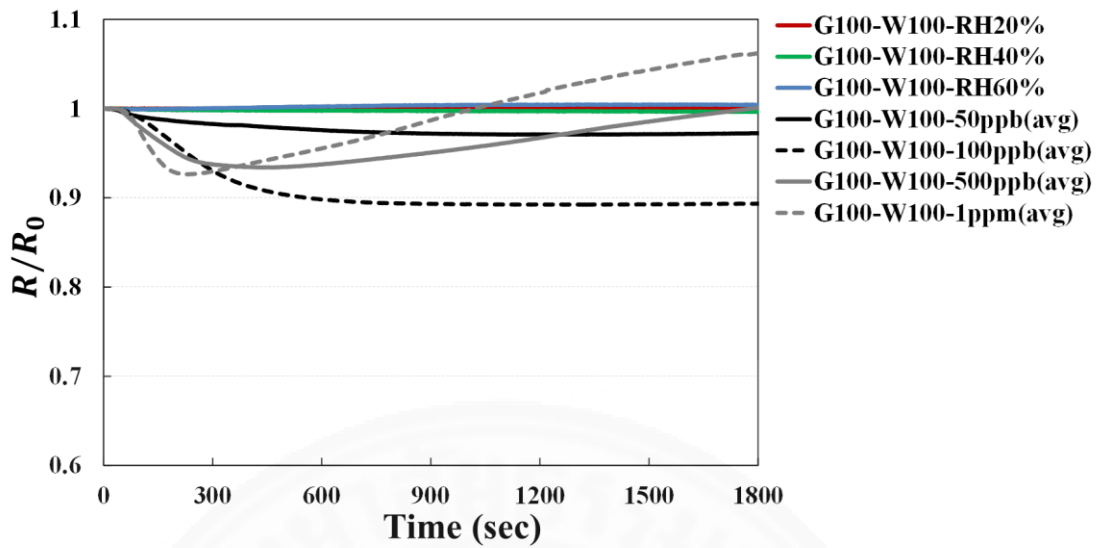


Figure 4.42 The responses of sensors to hydrogen sulfide compare to humidity. The humidity was varied: 20%, 40%, and 60%. Hydrogen sulfide gas was varied: 50 ppb, 100 ppb, 500 ppb, and 1 ppm. The gap between the electrodes is 100 μm (G100). The sensing wire is 100 μm (W100).

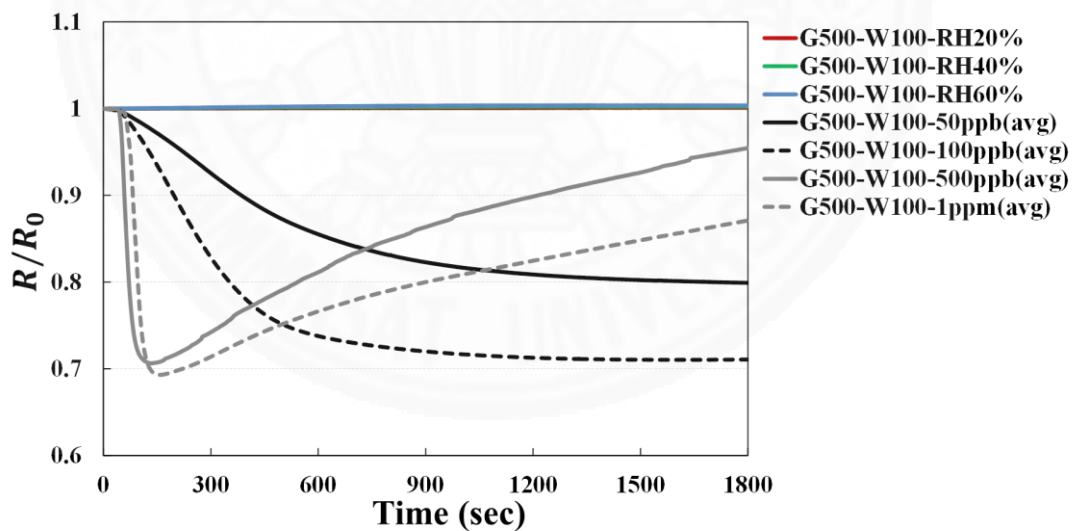


Figure 4.43 The responses of sensors to hydrogen sulfide compare to humidity. The humidity was varied: 20%, 40%, and 60%. Hydrogen sulfide gas was varied: 50 ppb, 100 ppb, 500 ppb, and 1 ppm. The gap between the electrodes is 500 μm (G500). The sensing wire is 100 μm (W100).

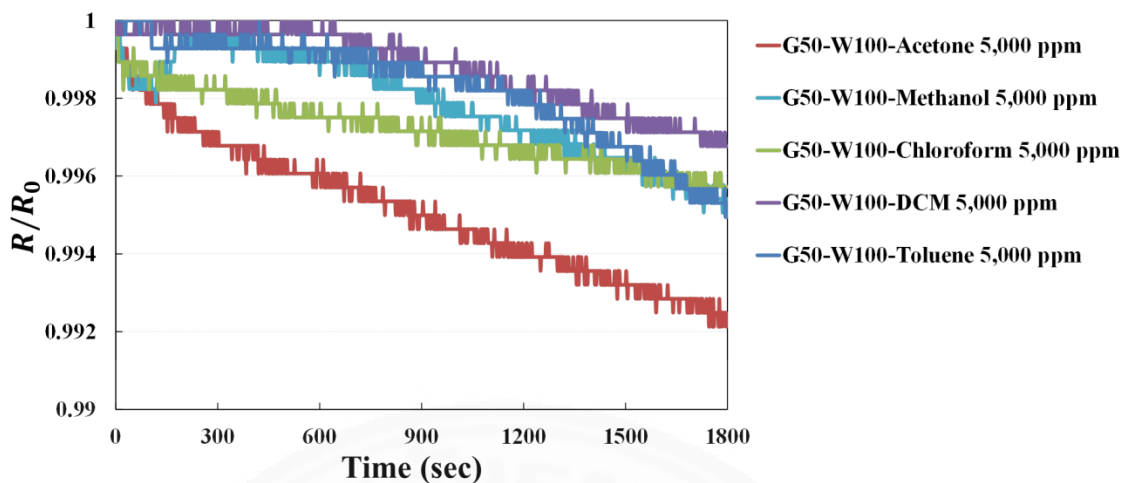


Figure 4.44 The responses of sensors to other gases: acetone, methanol, chloroform, dichloromethane (DCM), and toluene at 5,000 ppm. The gap between the electrodes is 50 μm (G50). The sensing wire is 100 μm (W100).

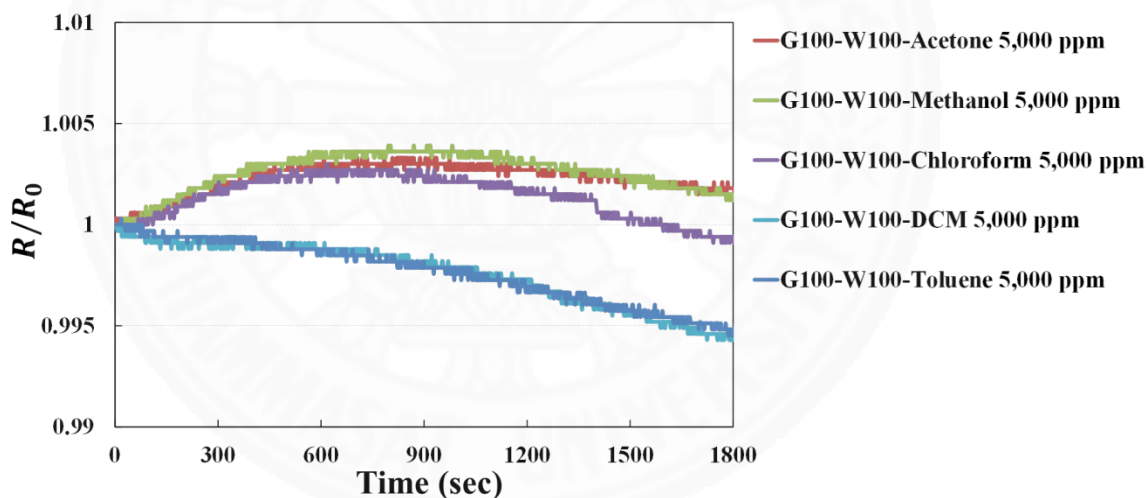


Figure 4.45 The responses of sensors to other gases: acetone, methanol, chloroform, dichloromethane (DCM), and toluene at 5,000 ppm. The gap between the electrodes is 100 μm (G100). The sensing wire is 100 μm (W100).

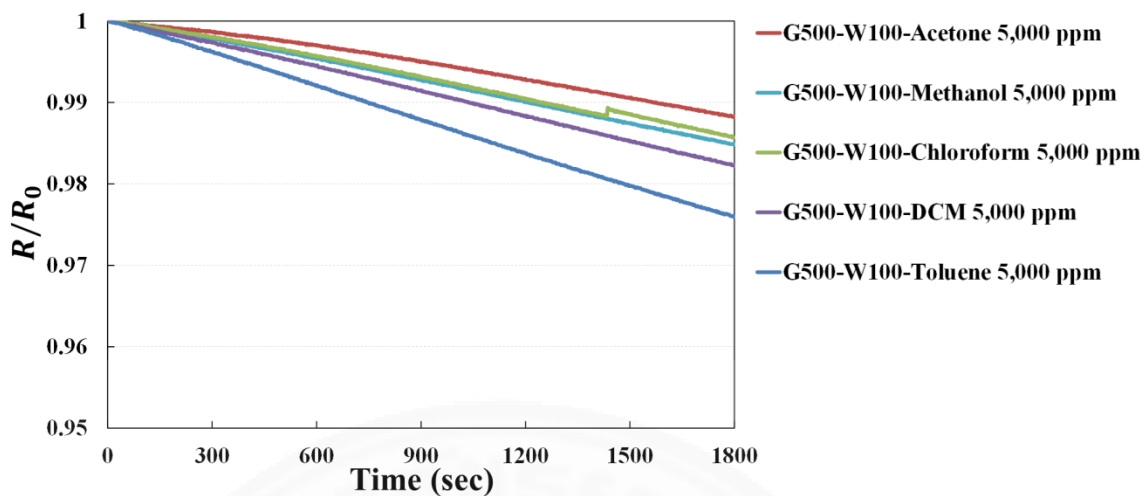


Figure 4.46 The responses of sensors to other gases: acetone, methanol, chloroform, dichloromethane (DCM), and toluene at 5,000 ppm. The gap between the electrodes is 500 μm (G500). The sensing wire is 100 μm (W100).

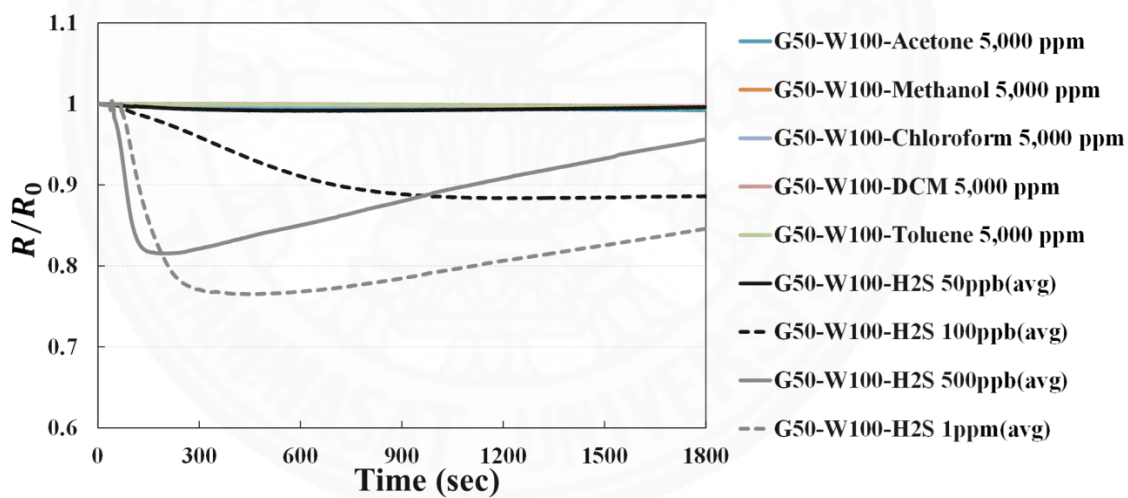


Figure 4.47 Responses of sensors (G50-W100) to hydrogen sulfide and other gases at time 30 min and ambient atmosphere. The concentration of hydrogen sulfide at 50 ppb, 100 ppb, 500ppb, 1,000 ppb(1 ppm) and the concentration of other gases at 5,000 ppm.

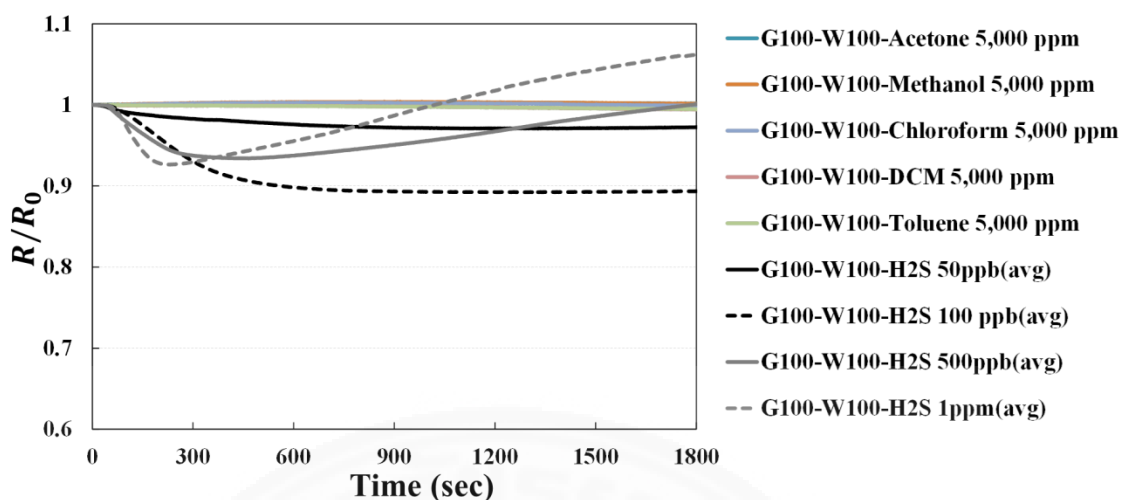


Figure 4.48 Responses of sensors (G100-W100) to hydrogen sulfide and other gases at time 30 min and ambient atmosphere. The concentration of hydrogen sulfide at 50 ppb, 100 ppb, 500ppb, 1,000 ppb(1 ppm) and the concentration of other gases at 5,000 ppm.

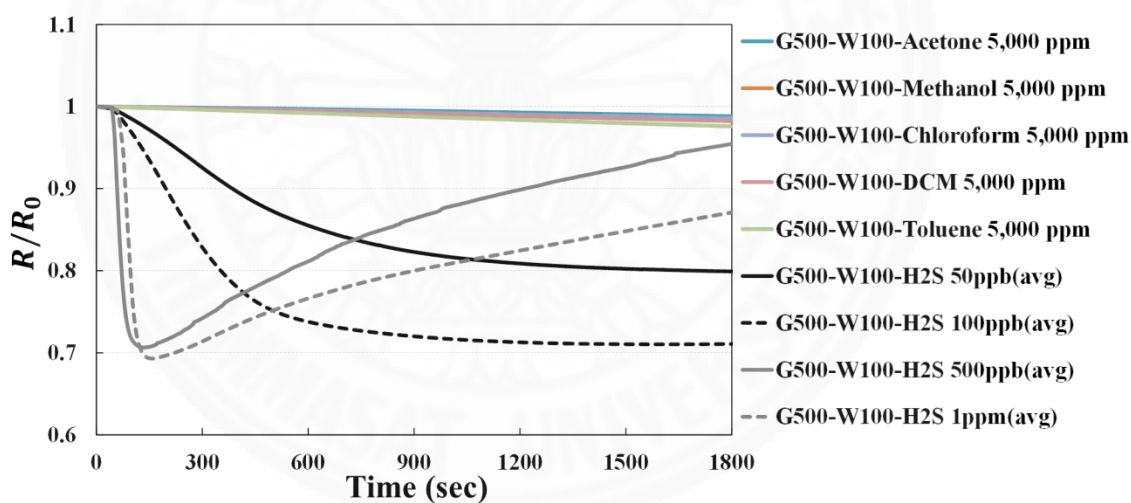


Figure 4.49 Responses of sensors (G500-W100) to hydrogen sulfide and other gases at time 30 min and ambient atmosphere. The concentration of hydrogen sulfide at 50 ppb, 100 ppb, 500ppb, 1,000 ppb(1 ppm) and the concentration of other gases at 5,000 ppm. This shows a very high selectivity of the developed silver nano-sensor towards hydrogen sulfide gas.

Figure 4.38 to Figure 4.43 show the responses of sensors to humidity. The humidity was varied: 20%, 40%, and 60%. The results show that the sensors respond to humidity

with various responses, but the responses are not significant when compare to the responses of sensor to hydrogen sulfide gas.

Figure 4.41 shows the comparison between the responses of sensors (G50-W100) to humidity and responses of sensors (G50-W100) to hydrogen sulfide at various concentrations. Therefore, humidity has no significant effects on sensors, except the response of the sensor G50-W100 (the one with narrowest gap) to hydrogen sulfide gas at 50 ppb concentration which has too weak response to hydrogen sulfide gas. In addition, the sensors also had high selectivity towards hydrogen sulfide gas compared to other gases as shown in Figure 4.47 to Figure 4.49. When the sensors were exposed to other gases, the resistances almost were not affected by the presence of other gases such as acetone, methanol, dichloromethane (DCM), toluene and chloroform, except the response of the sensor G50-W100 to hydrogen sulfide gas at 50 ppb concentration. The response of the sensor G50-W100 to hydrogen sulfide gas at 50 ppb has a weak signal with the intensity of the signal rather close to other gases and humidity.

From these results, it can be seen that the sensor G500-W100 is the best sensor for detecting hydrogen sulfide at various concentrations: from ppb to ppm range because the responses of sensor G500-W100 to hydrogen sulfide gas is higher than other sensors as G50-W100 and G100-W100. Moreover, when sensor G500-W100 was exposed to humidity and other gases, the results show that interferences from other gases have no have significant effects on the sensor G500-W100.

Chapter 5

Conclusion and recommendations

5.1 Conclusions

Sensor for detecting environmental toxic hydrogen sulfide gas has been developed based on the use of silver deposited onto silicon substrate. The silver deposited into micron-sized channel makes its resistance very sensitive to low concentration of hydrogen sulfide gas, and can detect the gas at concentration as low as 50 ppb within less than a minute of exposure. Concentrations range of hydrogen sulfide that the sensor fabricated in this work can detect is as low as 50 ppb and up to 500 ppm but higher concentrations should present no problem for detection. Lower concentration should also be possible using smaller channel.

The developed silver nanostructured sensor also has high selectivity response towards hydrogen sulfide, while other gases such as acetone, methanol, dichloromethane and toluene, showed almost no response especially when compared to that of hydrogen sulfide even the concentration of hydrogen sulfide gas very low concentration as 50 ppb. This silver nanostructured sensor can therefore be useful as an air quality monitoring tool that is specific to hydrogen sulfide in areas where the gas may be present such as wastewater treatment plant, landfills, farms, and industrial areas.

5.2 Recommendations

Fabrication process

Photoresists used for creating the sensor pattern should always be kept fresh. Old photoresists affect shape of the sensor pattern and the border roughness which might have an effect on the sensor reproducibility.

Silver nanostructured sensor

Refer to the long term stability of sensors, the sensors kept in ordinary case still show good performance even after one month of storage in a simple plastic

case. However the case should keep avoid sulfur gas compound. The gap between the electrodes can affect resistivity of the sensors. In addition, the thickness of the silver nanostructured sensing part also effects on the resistivity of sensors. Therefore, they need to be studied for having better responses at lower concentration in the ppb range.

Regeneration process

It is better if the sensors can be regenerated for reuse. Therefore, the silver nanostructured sensors may be regenerated for reuse by using thermal heating at temperature higher than 400 ° C. However, upon regeneration, the delicate nanostructured sensor might lose some properties. Therefore, further studies can also be made in this direction.

References

1. Choi, S.-W., et al., *Electrospun nanofibers of CuOSnO₂ nanocomposite as semiconductor gas sensors for H₂S detection*. *Sensors and Actuators B: Chemical*, 2013. **176**(0): p. 585-591.
2. Jiang, Z., P. Qin, and T. Fang, *Investigation on adsorption and decomposition of H₂S on Pd (1 0 0) surface: A DFT study*. *Surface Science*, 2015. **632**: p. 195-200.
3. Esfandyarpour, B., et al., *Ultrahigh-sensitive tin-oxide microsensors for H₂S detection*. *IEEE Sensors Journal*, 2004. **4**(4): p. 449-454.
4. Liang, X., et al., *Ultrasensitive and ultraselective detection of H₂S using electrospun CuO-loaded In₂O₃ nanofiber sensors assisted by pulse heating*. *Sensors and Actuators B: Chemical*, 2015. **209**: p. 934-942.
5. Hosseini, Z.S., A.I. zad, and A. Mortezaali, *Room temperature H₂S gas sensor based on rather aligned ZnO nanorods with flower-like structures*. *Sensors and Actuators B: Chemical*, 2015. **207, Part A**(0): p. 865-871.
6. Ryhl-Svendsen, M., *Corrosivity measurements of indoor museum environments using lead coupons as dosimeters*. *Journal of Cultural Heritage*, 2008. **9**(3): p. 285-293.
7. Ankersmit, H.A., N.H. Tennent, and S.F. Watts, *Hydrogen sulfide and carbonyl sulfide in the museum environment—Part 1*. *Atmospheric Environment*, 2005. **39**(4): p. 695-707.
8. Nisaratanaporn, E., et al., *Study on the microstructure, mechanical properties, tarnish and corrosion resistance of sterling silver alloyed with manganese*. *Materials Science and Engineering: A*, 2007. **445–446**: p. 663-668.
9. Liang, C., C. Yang, and N. Huang, *Tarnish protection of silver by octadecanethiol self-assembled monolayers prepared in aqueous micellar solution*. *Surface and Coatings Technology*, 2009. **203**(8): p. 1034-1044.

10. Pandey, S.K., K.-H. Kim, and K.-T. Tang, *A review of sensor-based methods for monitoring hydrogen sulfide*. TrAC Trends in Analytical Chemistry, 2012. **32**(0): p. 87-99.
11. Wetchakun, K., et al., *Semiconducting metal oxides as sensors for environmentally hazardous gases*. Sensors and Actuators B: Chemical, 2011. **160**(1): p. 580-591.
12. Chowdhuri, A., V. Gupta, and K. Sreenivas, *Fast response H₂S gas sensing characteristics with ultra-thin CuO islands on sputtered SnO₂*. Sensors and Actuators B: Chemical, 2003. **93**(1–3): p. 572-579.
13. Kaur, M., et al., *H₂S sensors based on SnO₂ films: RGTO verses RF sputtering*. Materials Chemistry and Physics, 2014. **147**(3): p. 707-714.
14. Shewale, P.S., et al., *H₂S gas sensitive Sn-doped ZnO thin films: Synthesis and characterization*. Journal of Analytical and Applied Pyrolysis, (0).
15. Verma, M., et al., *Comparison of H₂S sensing response of hetero-structure sensor (CuO–SnO₂) prepared by rf sputtering and pulsed laser deposition*. Thin Solid Films, 2010. **518**(24, Supplement): p. e181-e182.
16. Van Toan, N., et al., *Scalable fabrication of SnO₂ thin films sensitized with CuO islands for enhanced H₂S gas sensing performance*. Applied Surface Science, 2015. **324**(0): p. 280-285.
17. Ramgir, N.S., et al., *Sub-ppm H₂S sensing at room temperature using CuO thin films*. Sensors and Actuators B: Chemical, 2010. **151**(1): p. 90-96.
18. Chen, R., H.R. Morris, and P.M. Whitmore, *Fast detection of hydrogen sulfide gas in the ppmv range with silver nanoparticle films at ambient conditions*. Sensors and Actuators B: Chemical, 2013. **186**(0): p. 431-438.
19. Services, U.S.D.o.H.a.H., *Toxicological Profile for Hydrogen Sulfide And Carbonyl Sulfide*. 2014, U.S.Department of Health and Human Services: USA.
20. Salas, B.V., et al., *H₂S Pollution and Its Effect on Corrosion of Electronic Components*. 2012, INTECH.
21. Minzari, D., et al., *Morphological study of silver corrosion in highly aggressive sulfur environments*. Engineering Failure Analysis, 2011. **18**(8): p. 2126-2136.

22. *Electrochemical sensors, in Hazardous Gas Monitors. p. 29-35.*
23. Hua, C.Y.Y.W.K., W. Xiang, and T. Lu, *Electrochemical H₂S sensor with H₂SO₄ pre-treated Nafion membrane as solid polymer eletrolyte. Sensors and Actuators B, 2002: p. 259-265.*
24. Liu, X., et al., *A Survey on Gas Sensing Technology Sensors, 2012. 12: p. 9635-9664.*
25. Yoon, H., *Current Trends in Sensors Based on Conducting Polymer Nanomaterials. Nanomaterials, 2013. 3: p. 524-548.*
26. Fine, G.F., et al., *Metal Oxide Semi-Conductor Gas Sensors in Environmental Monitoring. Sensors, 2010. 10: p. 5470-5502.*
27. Kim, W.M., et al., *Effect of oxygen content and deposition temperature on the characteristics of thin silver films deposited by magnetron sputtering. Applied Surface Science, 2010. 257(4): p. 1331-1336.*
28. Rui, C., et al., *Silver sulfide nanoparticle assembly obtained by reacting an assembled silver nanoparticle template with hydrogen sulfide gas. Nanotechnology, 2008. 19(45): p. 455604.*
29. Liang, X., et al., *Ultrasensitive and ultraselective detection of H₂S using electrospun CuO-loaded In₂O₃ nanofiber sensors assisted by pulse heating. Sensors and Actuators B: Chemical, (0).*